



## **Porous Materials for Hydrogen Storage**

Zhijie Chen,<sup>1</sup> Kent O. Kirlikovali,<sup>1</sup> Karam B. Idrees,<sup>1</sup> Megan C. Wasson,<sup>1</sup> and Omar K. Farha<sup>1,2,\*</sup>

<sup>1</sup> Department of Chemistry and International Institute for Nanotechnology, Northwestern University, 2145 Sheridan Road, Evanston, Illinois 60208, United States

<sup>2</sup> Department of Chemical & Biological Engineering, Northwestern University, Evanston, Illinois 60208, United States

\*Corresponding author / Lead contact. Email: o-farha@northwestern.edu

# **MAIN TEXT**

## **SUMMARY**

The development of efficient storage materials for hydrogen is important for the viable implementation of hydrogen-powered fuel cell automobiles. In this review, we summarize progress towards the development of state-of-the-art porous materials, including metal–organic frameworks (MOFs), covalent organic frameworks, porous organic polymers, carbon-based materials, and zeolites, for hydrogen storage. In particular, we illustrate the fundamental considerations for the targeted design and synthesis of MOFs with better hydrogen storage performance aided by reticular chemistry and a simulation-aid strategy. Additionally, we highlight some progress related to porous material-based composites with encapsulated hydrides of light elements (HLEs). Finally, we provide an outlook for the future path of porous materials as a viable technology for hydrogen storage, including the discovery of materials with improved gravimetric and volumetric storage capacities at ambient temperatures, the engineering of materials into practical gas vessels, and future commercialization.

## **1. Introduction**

The current global energy supply primarily relies on fossil fuels, including coal, oil, and natural gas.<sup>1</sup> These traditional energy sources have empowered humans with extraordinary agricultural and industrial technological capabilities since the dawn of the industrial revolution; however, environment-related issues that result from the consumption of fossil fuels are increasingly raising public concerns about global climate change.<sup>2</sup> In 2013, the global average atmospheric carbon dioxide concentration reached an unprecedented 400 parts per million (ppm) and has continued to increase since then.<sup>3</sup> With continuous population and economic growth, the world's energy consumption is projected to grow rapidly and can lead to further environmental and climate risks.<sup>2,4</sup> To that end, the transformation of existing fossil fuels to alternative, diversified energy sources that are affordable, obtainable, and renewable is of great importance in both the near- and long-term. Among these potential energy sources, hydrogen is considered a clean and sustainable energy carrier capable of realizing a carbon-neutral energy cycle and envisioned as the “fuel of the future”.<sup>5-8</sup> Since water is the only by-product that forms during the consumption of hydrogen as an energy supply, the world-wide usage of hydrogen in fuel cell

cars could mitigate challenges related to the emission of greenhouse gases and air pollution that face our planet today.

With the chemical formula  $H_2$ , hydrogen is one of the simplest molecules known and possesses a much higher gravimetric, yet lower volumetric energy density, compared to gasoline ( $120 \text{ MJ kg}^{-1}$  and  $8 \text{ MJ L}^{-1}$  for liquid hydrogen versus  $44 \text{ MJ kg}^{-1}$  and  $32 \text{ MJ L}^{-1}$  for gasoline).<sup>9</sup> Despite this favorable energy density, an efficient hydrogen storage system is one of the major technological barriers that limits the development and large-scale commercialization of zero-emission hydrogen-powered fuel cell vehicles.<sup>10</sup> In order to achieve practical driving ranges for automobiles comparable to that of gasoline-powered vehicles, the current established technologies for on-board hydrogen storage mainly rely on compressed gas or liquified gas tanks to attain reasonable energy densities. Compressed hydrogen requires the use of expensive and potentially unsafe type IV carbon fiber-reinforced composite tanks to load hydrogen up to about 700 bar.<sup>6,11</sup> In contrast, liquid hydrogen tanks are refrigerated at a temperature of  $\sim 20 \text{ K}$  to liquify hydrogen at atmospheric pressure. In both cases, these approaches are complicated and costly, and their extreme operating conditions raise safety concerns that currently limit the implementation of hydrogen in transportation-related applications.<sup>11</sup>

In this regard, hydrogen storage materials that aim to reduce the operational pressures while also maintaining the high storage capacities of hydrogen offer an alternative solution to these conventional technologies.<sup>11</sup> In order to inspire the development of materials for on-board hydrogen storage in light-duty automobiles, the US Department of Energy (DOE) set system-level technical hydrogen storage targets of 5.5 wt % and  $40 \text{ g L}^{-1}$  by 2025 and an ultimate target of 6.5 wt % and  $50 \text{ g L}^{-1}$ .<sup>12</sup> These targets describe usable storage capacities under the related operating conditions. Over the past two decades, solid-state porous materials and their related composites have stood out as promising candidates in the context of hydrogen storage materials due to their unique characteristics, including functionalizable pore environments, significant tunability, and large, accessible surface areas and high porosities. In particular, researchers have widely studied metal–organic frameworks (MOFs),<sup>13–16</sup> covalent organic frameworks (COFs),<sup>17–19</sup> porous organic polymers (POPs),<sup>20,21</sup> carbon-based materials,<sup>22</sup> zeolites,<sup>23</sup> and their related composites<sup>8,24</sup> with encapsulated hydrides of light elements (HLEs) for hydrogen storage applications.

The objective of this review is to provide an overview of recent progress in the development of porous materials for hydrogen storage, as well as to offer proposed guidelines to develop even better hydrogen storage materials. Specifically, we will highlight representative examples that employ both experimental and theoretical approaches to develop advanced hydrogen storage MOFs, beginning with an emphasis on the importance of reticular chemistry for the design and synthesis of these frameworks. Precise molecular-level control enabled by a reticular approach is essential to fine-tune the porous MOF structures for desired applications and will act as an important tool for the design of even better storage materials in the future. Next, we will detail examples of high-throughput simulations that can identify potential MOF materials with high hydrogen storage capacities. Additionally, we will highlight MOFs that exhibit balanced gravimetric and volumetric hydrogen storage capacities, as well as MOFs that aim to store hydrogen at ambient temperature, and we will summarize the progress of other adsorbents, such as COFs, POPs, carbon-based materials, and zeolites for hydrogen storage. We will touch on the advantages and drawbacks of HLEs and highlight representative examples of promising hybrid systems that contain HLEs encapsulated in porous materials for hydrogen storage. Finally, we will offer our thoughts for future prospects in the context of materials design, process engineering, and commercialization of porous materials for hydrogen storage. We hope that this review will provide young researchers in particular with an overview in the application of porous materials and their related composites to hydrogen storage, as well as inspire efforts towards the development of next-generation hydrogen storage materials required for the eventual realization of a carbon-neutral energy cycle.

## **2. MOF adsorbents for hydrogen storage**

### **2.1 A brief overview of MOFs for hydrogen storage**

Metal–organic frameworks (MOFs) are a class of porous framework materials assembled from inorganic building units (i.e., metal ions or clusters) and organic ligands via coordination bonds.<sup>25,26</sup> The exploration of MOFs for use in hydrogen storage applications has been ongoing for nearly two decades since the pioneering example by the Yaghi group in 2003.<sup>13</sup> In recent years, however, there has been significant progress regarding the design and synthesis of MOFs for hydrogen storage from both experimental and theoretical perspectives. For example, highly

porous MOFs display impressive gravimetric and volumetric hydrogen deliverable capacities under combined temperature and pressure swing conditions.<sup>27,28</sup> Other examples leverage strong backbonding interactions between hydrogen molecules and exposed low-valent metals in the nodes, such as Cu(I) and V(II), to enhance the binding energy between the MOF and H<sub>2</sub> that leads to improved hydrogen storage capacities at ambient temperatures.<sup>29,30</sup> In addition, theoretical strategies have emerged in which researchers can computationally screen databases that contain nearly half a million real and hypothetical MOFs to identify materials that might exhibit outstanding hydrogen storage performance<sup>28</sup> or apply machine learning methods to accelerate the discovery of MOF candidates that are predicted to be excellent candidates for hydrogen storage.<sup>31</sup> Despite numerous successful examples from these strategies, the use of MOFs as practical on-board hydrogen storage systems remains a challenging opportunity due to the requirement for balanced gravimetric and volumetric storage capacities at ambient temperature, system-level operation, and cost.

In this part, we summarize some of the representative examples regarding the design and synthesis of MOFs for hydrogen storage (**Figure 1**). It is worth noting that the deliverable capacity at a certain temperature is defined as the difference between the uptake at the maximum refueling pressure (e.g, 100 bar) and the uptake at the minimum delivery pressure (e.g, 5 bar). 100 bar is suggested as the highest loading pressure because relatively inexpensive, all-metal type I pressure vessels can be safely applied at this pressure, and the type IV carbon fiber-reinforced composite tanks do not need to be employed.<sup>11,32</sup> The deliverable hydrogen capacity can be maximized when using a combined temperature and pressure swing operational condition (77 K/100 bar → 160 K/5 bar), which is from the tank design proposed by the DOE center Hydrogen Storage Engineering Center of Excellence.<sup>33</sup> Additionally, if not specified, the volumetric hydrogen uptakes for MOFs in this review are calculated based on crystallographic density, which are obtained from literature, or calculated using a geometry-optimized computational approach.

## 2.2 Reticular chemistry and molecular simulation

Currently, hydrogen storage in MOFs primarily relies on the inherent pore size, pore environment, pore volume, and surface area of the MOF. Both the rational design and precise

synthesis of targeted MOFs with a desired pore geometry and functionality are vital for the development and discovery of better storage materials for hydrogen. Pioneering work from Yaghi and coworkers revealed the extended MOFs such as MOF-210 with larger pore volumes and surface areas show better total hydrogen uptakes at 77 K than MOF-177.<sup>34,35</sup> Reticular chemistry enables the architectural assembly of framework-type materials by connecting the pre-chosen building units with the aid of blueprint topological networks.<sup>36-40</sup> In particular, edge-transitive nets with only one type of net are among the most prominent networks for the design and synthesis of MOFs, and this reticular chemistry approach has been widely deployed to design and synthesize porous MOFs based on edge-transitive nets for diverse applications, ranging from gas separation<sup>41,42</sup> to methane and hydrogen storage.<sup>43,44</sup> One of the early examples in this field involves the reticular extension of rht-MOFs<sup>45-47</sup> to the *de novo* synthesis of an ultraporous MOF with the 3,24-connected **rht** net, NU-100, which exhibits excellent hydrogen storage performance.<sup>44</sup> The ability for researchers to control the assembly of MOFs at the molecular level *via* the use of reticular chemistry will continue to empower the synthesis of better hydrogen storage materials.

Apart from the precise synthesis aided by reticular chemistry, large-scale molecular simulation is another important tool that allows researchers to identify potential MOF candidates best suited for hydrogen storage. For example, Snurr and coworkers pioneered the use of a computational approach to generate a large number of hypothetical MOFs, and from this set, identified promising candidates for gas storage *via* large-scale screening.<sup>48-50</sup> Molecular simulation often accelerates the selection of candidate MOF materials, which can be previously reported or hypothetical, for hydrogen storage. Siegel and coworkers applied grand canonical Monte Carlo (GCMC) simulations to predict MOFs that would exhibit better usable capacities than that of MOF-5 under relevant operating conditions for on-board storage systems (77 K/100 bar  $\rightarrow$  160 K/5 bar).<sup>51</sup> The combined simulation and experimental results from this study revealed that IRMOF-20, an isorecticular extended structure of MOF-5, shows a better gravimetric, yet a slightly lower volumetric, H<sub>2</sub> working capacity compared to those of MOF-5 (9.1 wt% versus 7.8 wt% and 51.0 g L<sup>-1</sup> versus 51.9 g L<sup>-1</sup>) under the aforementioned operating conditions. They further computationally screened nearly half a million MOF structures to identify high-capacity MOF materials for hydrogen storage, and among these, PCN-610/NU-100 emerged as a promising candidate with an experimental H<sub>2</sub> usable capacity of 13.9 wt% and 47.6

g L<sup>-1</sup> under a combined temperature and pressure swing condition between 100 bar/77 K and 5 bar/160 K.<sup>28</sup> Recently, the Snurr group reported a combined machine learn prediction and GCMC simulation approach to accelerate screening of MOFs for hydrogen storage. One of the best candidates identified using this strategy – MFU-4l – displays an excellent experimental volumetric hydrogen deliverable capacity when operating at a combined temperature and pressure swing condition (77 K/100 bar → 160 K/5 bar).<sup>31</sup>

Once a MOF that is based on a specific topological net is identified by high-throughput computational screening, the application of reticular chemistry as a practical synthetic tool is crucial to rationally synthesize the targeted MOF. For example, PCN-224<sup>52</sup> with the 4,6-connected edge-transitive **she** net is based on 4-connected square organic linkers and 6-connected Zr<sub>6</sub> nodes. A high-throughput model identified this topological net as potentially favorable for hydrogen storage, and reticular chemistry enabled the synthesis of a series of isorecticular **she**-MOFs to validate this prediction.<sup>53</sup> These **she**-MOFs are comprised of 4-connected square copper paddlewheel building units and 6-connected hexagonal organic ligands, and this representative example highlights the power of reticular chemistry as it enables access to designed, reticular materials that are based on the same underlying nets but assembled from different chemical building blocks. The marriage of reticular chemistry and molecular simulation will continue to facilitate the discovery and subsequent synthesis of high-performance MOF materials towards hydrogen storage.

### 2.3 Highly porous MOFs for cryo-adsorbed hydrogen storage

Highly porous MOFs are promising candidates for hydrogen storage due to their high accessible surface areas and porosities, particularly at cryo-temperatures such as 77 K. Apart from the highly porous MOFs based on Cu<sub>2</sub> and Zn<sub>4</sub> clusters discussed in the previous section (i.e., Cu-**she**-MOFs, IRMOF-20, and NU-100), we give an overview of some representative examples of stable MOFs based on high-valent metal clusters, such as Zr<sub>6</sub>, Al<sub>3</sub>, and Fe<sub>3</sub> building units, and carboxylate linkers for hydrogen storage (**Table 1** and **Figure 2**). The strong coordination bonds that form between these high-valent metal nodes and carboxylate groups in the linkers impart exceptional stability to these MOFs, which is required for the implementation of these materials in gas tanks.

Gómez-Gualdrón *et al.* applied both experimental and computational methods to study a series of highly stable zirconium-based MOFs (Zr-MOFs), NU-1101, NU-1102 and NU-1103, for cryo-adsorbed hydrogen storage to understand the trade-off between gravimetric and volumetric usable capacities.<sup>54</sup> These Zr-MOFs are assembled from  $Zr_6$  clusters and tetracarboxylate linkers and based on the highly connected 4,12-connected **ftw** net, and they show very high Brunauer–Emmett–Teller (BET) areas that range from  $3720\text{ m}^2\text{ g}^{-1}$  to  $6245\text{ m}^2\text{ g}^{-1}$ . Experimental hydrogen adsorption measurements revealed that NU-1103, which exhibits a BET area of  $6245\text{ m}^2\text{ g}^{-1}$ , displays a high gravimetric deliverable uptake of 12.6 wt% ( $43.2\text{ g L}^{-1}$ ) under the pressure and temperature swing operating conditions (77 K/100 bar  $\rightarrow$  160 K/5 bar). In comparison, NU-1101 (BET area:  $4340\text{ m}^2\text{ g}^{-1}$ ) and NU-1102 (BET area:  $3720\text{ m}^2\text{ g}^{-1}$ ) show slightly higher volumetric usable capacities of  $46.6\text{ g L}^{-1}$  (9.1 wt%) and  $43.7\text{ g L}^{-1}$  (9.6 wt%), respectively. Recently, Chen, Zhou, Zhang, and coworkers reported empirical equations they obtained from previous experimental data to predict the highly porous and stable Zr-MOF, NPF-200, as an effective MOF for cryo-adsorbed hydrogen storage at 77 K.<sup>55</sup> NPF-200 is a cage-type MOF with a BET area of  $5830\text{ m}^2\text{ g}^{-1}$  ( $2268\text{ m}^2\text{ cm}^{-3}$ ) built from the assembly of  $Zr_6$  clusters and tetrahedral carboxylate ligands. Hydrogen adsorption experiments revealed a very high volumetric deliverable capacity of  $37.2\text{ g L}^{-1}$  (8.7 wt%) under the operating conditions (77 K/100 bar  $\rightarrow$  77 K/5 bar) for NPF-200, validating this predictive method.

Recently, our group reported the rational design and synthesis of a highly porous MOF platform – NU-1500 – from the assembly of trigonal prismatic ligands and metal trimer-based  $Al_3O$  and  $Fe_3O$  building units.<sup>57</sup> NU-1500 is based on the 6-connected edge transitive **acs** net and is amenable to isorecticular expansion, and NU-1500-Al demonstrates a BET area of  $3560\text{ m}^2\text{ g}^{-1}$  and a deliverable  $H_2$  capacity of  $44.6\text{ g L}^{-1}$  (8.2 wt%) under the operating condition (77 K/100 bar  $\rightarrow$  160 K/5 bar).<sup>27</sup> The reasonably high volumetric capacity and moderate gravimetric capacity motivated us to further explore the trade-off between gravimetric and volumetric deliverable  $H_2$  capacity for this **acs**-MOF platform under the previously mentioned operating conditions, so we conducted molecular simulations based on a database containing 2800 MOFs.<sup>27</sup> The structure-property relationship from molecular simulations revealed that NU-1501, which is an isorecticular analogue of NU-1500 based on the same metal trimers and extended ligands that contain one additional phenyl group in each arm of the linker, was at the ideal region that balanced gravimetric and volumetric deliverable  $H_2$  capacities. We applied reticular

chemistry to precisely design and synthesize this class of targeted MOF materials, including NU-1501-Al and NU-1501-Fe. Based on calculations from the N<sub>2</sub> adsorption isotherm, NU-1501-Al displays a gravimetric BET area of 7310 m<sup>2</sup> g<sup>-1</sup> after fulfilling four BET consistency criteria.<sup>58,59</sup> Importantly, NU-1501-Al shows a very high H<sub>2</sub> deliverable capacity of 14.0 wt% while maintaining a reasonably high volumetric deliverable capacity of 46.2 g L<sup>-1</sup> under the operating conditions (77 K/100 bar → 160 K/5 bar). Interestingly, the highly porous NU-1501-Al can adsorb ~2.9 wt% (~8.4 g L<sup>-1</sup>) of H<sub>2</sub> at 296 K and 100 bar, and this gravimetric uptake is much higher than the values of most reported MOFs under these conditions. In addition, the isoreticular NU-1501-Fe analogue that is based on iron trimers shows similarly high H<sub>2</sub> capacity, illustrating the generality of outstanding hydrogen storage performance for this MOF platform.

Recently, we reported the enhancement of hydrogen capacity of a robust azolate-based MOF via a post-synthetic modification strategy.<sup>56</sup> MFU-4l-Li, obtained from the post-synthetic treatment of MFU-4l based on triazolate-based ligands and Zn<sub>5</sub> nodes, displays an improved storage capacity towards hydrogen than the parent MOFs. Under the operating condition (77 K/100 bar → 160 K/5 bar), MFU-4l-Li shows an impressive deliverable capacity of 50.2 g L<sup>-1</sup> and 9.4 wt% for H<sub>2</sub>, which are higher than those values of MFU-4l (44.3 g L<sup>-1</sup> and 7.3 wt%). Such increase of the hydrogen storage performance can be attributed to the enhancement of pore volume and surface area after the post-synthetic modification.

## 2.4 MOFs for hydrogen storage at ambient temperature

Generally, hydrogen can only weakly interact with the surfaces of MOF materials due to its low polarizability and the lack of interactions between hydrogen and most MOFs. For example, the highly porous MOFs described in previous sections display isosteric heats of adsorption ( $Q_{st}$ ) of about -5 kJ mol<sup>-1</sup> due to weak interactions with H<sub>2</sub>, so cryogenic temperatures are essential to achieve reasonable hydrogen capacities and to supply satisfactory driving ranges in fuel cell vehicles when using adsorption-based hydrogen storage technology. The ideal  $Q_{st}$  range of hydrogen in MOFs is believed to be between -15 and -25 kJ mol<sup>-1</sup>; this domain represents efficient hydrogen storage capacity at room temperature under automobile-relevant conditions,<sup>60-62</sup> but the values of hydrogen binding enthalpies for most MOFs are less than -8 kJ mol<sup>-1</sup>.<sup>16</sup> Therefore, one strategy to enhance hydrogen storage in MOFs at ambient temperatures

focuses on increasing the hydrogen binding affinity of the MOFs while maintaining high surface areas and porosities.

Enhancing the charge density of MOFs has been reported as an efficient approach to improve the interactions between H<sub>2</sub> and MOFs. For example, Eddaoudi and coworkers studied a series of M-**soc**-MOFs with different inorganic trinuclear clusters (i.e., In<sup>3+</sup> and Fe<sup>3+</sup>) and counterions (i.e., NO<sub>3</sub><sup>-</sup>, Cl<sup>-</sup> and Br<sup>-</sup>) for H<sub>2</sub> sorption.<sup>63,64</sup> Highly localized charge density, as well as favorable pore sizes and geometries result in the strong interactions between **soc**-MOFs and H<sub>2</sub>, as evidenced by a high H<sub>2</sub> Q<sub>st</sub> of -7.9 kJ mol<sup>-1</sup> for Fe-**soc**-MOF-1a with a NO<sub>3</sub><sup>-</sup> counterion. In another example, Chen, Thomas and coworkers reported that a MOF with a narrow pore size of less than 0.56 nm maximizes the interactions between H<sub>2</sub> and open copper sites, displaying a high H<sub>2</sub> Q<sub>st</sub> of -12.3 kJ mol<sup>-1</sup>.<sup>65</sup> Similarly, Zhou *et al.* systematically studied a series of M-MOF-74 (M = Mg, Mn, Co, Ni, Zn) with open metal sites for H<sub>2</sub> adsorption.<sup>66</sup> M-MOF-74<sup>67</sup> is also known as CPO-27-M<sup>68</sup> and M<sub>2</sub>(dobdc), where dobdc<sup>4-</sup> refers to 2,5-dioxido-1,4-benzenedicarboxylate. These experimental results revealed that the Q<sub>st</sub> of H<sub>2</sub> for M-MOF-74, which contains transition metal ions in similar coordination environments, follows the trend of Zn-MOF-74 < Mn-MOF-74 < Mg-MOF-74 < Co-MOF-74 < Ni-MOF-74.<sup>66</sup> This trend of H<sub>2</sub> binding can be empirically predicted by the radius of the transition metal ion and is consistent with the Irving–Williams series<sup>69</sup>, which empirically describes the order of stability of high spin transition metal complexes.

In order to further increase charge density of MOFs and improve their H<sub>2</sub> binding strengths, Long and coworkers synthesized a series of structural isomers of MOF-74, M<sub>2</sub>(*m*-dobdc), where *m*-dobdc<sup>4-</sup> is 4,6-dioxido-1,3-benzenedicarboxylate (**Figure 3**).<sup>70</sup> Experimental results revealed M<sub>2</sub>(*m*-dobdc) (M= Ni, Co, Fe, Mn and Mg), which consist of open metal sites with enhanced charge density, have higher H<sub>2</sub> binding enthalpies relative to those of M-MOF-74, due to the modification of the ligand field at the metal sites. The Q<sub>st</sub> of H<sub>2</sub> for Ni<sub>2</sub>(*m*-dobdc) and Co<sub>2</sub>(*m*-dobdc) at low loadings are -12.3 kJ mol<sup>-1</sup> and -11.5 kJ mol<sup>-1</sup>, respectively, which are higher than those of Ni<sub>2</sub>(dobdc) (-11.9 kJ mol<sup>-1</sup>) and Co<sub>2</sub>(dobdc) (-10.8 kJ mol<sup>-1</sup>). The overall trend for the H<sub>2</sub> binding strength for M<sub>2</sub>(*m*-dobdc) matches well with the Irving–Williams series<sup>69</sup>, similar to that of M<sub>2</sub>(dobdc). The authors combined a variety of spectroscopic tools (e.g., powder neutron and X-ray diffraction, inelastic neutron scattering and infrared spectroscopy) with computational simulations to understand the relationship between the structural

modifications and the enhancement in H<sub>2</sub> adsorption properties. For example, neutron diffraction experiments revealed that the distance between the center of electron density for D<sub>2</sub> and the metal center at the primary binding site is 2.23(5) Å for Co<sub>2</sub>(*m*-dobdc), which is shorter than that of Co<sub>2</sub>(dobdc), 2.32(2) Å, and suggests stronger metal-H<sub>2</sub> interactions for Co<sub>2</sub>(*m*-dobdc) than Co<sub>2</sub>(dobdc). The team conducted additional high-pressure hydrogen adsorption studies and revealed that this class of MOFs shows very good volumetric H<sub>2</sub> capacities at near-ambient temperatures, as exemplified by a working capacity of 11.0 g L<sup>-1</sup> between 100 bar and 5 bar at 298 K for Ni<sub>2</sub>(*m*-dobdc). However, the gravimetric hydrogen storage performance of these MOFs needs further improvement to be considered for practical on-board hydrogen storage applications.<sup>71</sup>

Apart from MOFs with high charge density, MOFs with low valent metal sites, which can interact with H<sub>2</sub> via  $\pi$ -backbonding, are also considered promising candidates for H<sub>2</sub> storage at ambient temperatures. We will highlight two MOFs with high H<sub>2</sub> binding enthalpies: Cu<sup>I</sup>-MFU-4l (-32 kJ mol<sup>-1</sup>)<sup>29</sup> and V<sub>2</sub>Cl<sub>2.8</sub>(btdd) (-21 kJ mol<sup>-1</sup>)<sup>30</sup>, where btdd refers to bis(1*H*-1,2,3-triazolo[4,5-*b*],[4',5'-*i*])dibenzo[1,4]dioxin (**Figure 4**). MFU-4l is a robust Zn-MOF assembled from ZnCl<sub>2</sub> and azolate-based ligands (btdd) and based on the edge-transitive 6-connected **pcu** net.<sup>72</sup> Cu<sup>II</sup>-MFU-4l can be obtained from the transmetalation of MFU-4l, and further treatment of Cu<sup>II</sup>-MFU-4l with a solution of lithium formate hydrate yields Cu<sup>II</sup>-MFU-4l-formate. Finally, heating Cu<sup>II</sup>-MFU-4l-formate under vacuum at 180 °C generates Cu<sup>I</sup>-MFU-4l, which contains trigonal pyramidal open Cu<sup>+</sup> sites.<sup>29</sup> The Q<sub>st</sub> of H<sub>2</sub> for Cu<sup>I</sup>-MFU-4l is -32 kJ mol<sup>-1</sup>, based on the calculation from adsorption isotherms at different temperatures using the Clausius–Clapeyron equation, and such high Q<sub>st</sub> suggests Cu<sup>I</sup>-MFU-4l chemisorbs H<sub>2</sub> *via* nondissociative hydrogen binding. In further mechanistic investigations, researchers observed a metastable physisorbed precursor intermediate during chemisorption process and emphasized the importance of studying kinetics of adsorption for the design of future hydrogen adsorbent.<sup>73</sup> Similarly, Long and coworkers recently successfully synthesized a vanadium-based MOF, V<sub>2</sub>Cl<sub>2.8</sub>(btdd), which contains  $\pi$ -basic low-valent V<sup>2+</sup> sites, from the assembly of vanadium salts and btdd.<sup>30</sup> Low-pressure gas adsorption experiments revealed V<sub>2</sub>Cl<sub>2.8</sub>(btdd) has a H<sub>2</sub> binding enthalpy of -21 kJ mol<sup>-1</sup>, and further mechanistic studies suggested a weak Kubas-type interaction between V<sup>2+</sup> sites and H<sub>2</sub> during adsorption. This Q<sub>st</sub> lies in the ideal range of hydrogen storage at ambient temperatures due to the backbonding from V<sup>2+</sup> into the  $\sigma^*$  orbital of dihydrogen. Indeed, high-

pressure H<sub>2</sub> adsorption experiments revealed V<sub>2</sub>Cl<sub>2.8</sub>(btdd) displays a high volumetric uptake of 10.7 g L<sup>-1</sup> at 298 K and 100 bar. Similar to Ni<sub>2</sub>(*m*-dobdc), V<sub>2</sub>Cl<sub>2.8</sub>(btdd) shows a moderate gravimetric H<sub>2</sub> uptake of 1.64 wt %.

Overall, these noteworthy studies on Cu<sup>I</sup>-MFU-4l and V<sub>2</sub>Cl<sub>2.8</sub>(btdd) revealed that MOFs comprise a class of promising materials for hydrogen storage at ambient temperatures, although the development of better MOF adsorbents with improved hydrogen capacities will require continued efforts. Optimal pore sizes and pore geometries, together with higher density of low-valent transition metal sites, could yield a MOF with a favorable H<sub>2</sub> binding enthalpy and optimal deliverable capacities at ambient temperatures.

### **3. Other adsorbents (i.e., COFs, POPs, carbon-based materials, and zeolites) for hydrogen storage**

#### *Other Physical Sorbents*

Beyond the use of MOFs as physical sorbents towards hydrogen storage, there has been a growing interest in the use of other materials, such as COFs, POPs, zeolites, and carbon-based materials, as hydrogen sorbents. Similar to MOFs, COFs and zeolites are porous solids with crystalline, ordered structures. On the other hand, POPs and carbon-based materials typically have amorphous structures, yet maintain permanent porosity. Similar to the MOFs described in previous sections, researchers are targeting the development of porous sorbents within these classes of materials to exhibit high H<sub>2</sub> uptake and affinity. In this section, we summarize the apparent advantages and disadvantages of these porous materials towards hydrogen storage (**Figure 5**).

#### *Covalent Organic Frameworks*

COFs are a class of porous, crystalline materials constructed from organic building units that are connected through covalent bonds to form two- or three-dimensional frameworks that exhibit good chemical and thermal stability.<sup>17-19</sup> Yaghi first reported the discovery of 2D COFs in 2005 and followed up with 3D COFs in 2007.<sup>17,77</sup> Advancements in both organic chemistry and reticular chemistry has enabled the formation of these porous, crystalline materials – as opposed to non-porous and amorphous organic solids – through controlled reaction conditions

and the thoughtful design of organic precursors. Extensive computational studies have investigated the use of COFs as hydrogen adsorbents owing to their large surface areas and pore volumes, as well as their ability to form low-density materials since they consist of light elements rather than the relatively heavier metals present in MOFs.<sup>78</sup>

Inspired by reticular chemistry, Yaghi and co-workers first synthesized three-dimensional COFs (3D-COFs) based on the **ctn** and **bor** nets<sup>77</sup> as these 3D-COF have been theorized as low-density alternatives to MOFs that do not contain open-metal sites.<sup>78</sup> If disregarding the impact of the open-metal sites of MOFs in hydrogen-framework interactions, a COF with a similar surface area to a MOF is expected to exhibit a comparable volumetric uptake but a significantly higher gravimetric uptake due to the relatively lower density of the COF.<sup>79</sup> In 2009, Furukawa and Yaghi studied the hydrogen adsorption on a series of seven porous COFs at 1–85 bar and 77–298 K and divided the systems into three groups based on their structural dimensions and corresponding pore sizes.<sup>80</sup> High-pressure H<sub>2</sub> isotherms for these COFs measured at 77 K showed a wide-range of saturation uptakes (surface excess amount): 14.8 and 22.6 mg g<sup>-1</sup> for group 1 (2D-COFs with small 1D pores), 35.8, 35.0, and 39.2 mg g<sup>-1</sup> for group 2 (2D-COFs with large 1D pores), and 72.4 and 70.5 mg g<sup>-1</sup> for group 3 (3D-COFs with medium 3D pores). At the time of publication, the authors found that group 3 (COF-102 and COF-103), were far better than the 2D-COFs and rivaled the best MOFs and other porous materials in their hydrogen uptake capacities. At 77 K, COF-103 displays a total deliverable uptake of 6.4 wt % (29.2 g L<sup>-1</sup>) for hydrogen when operating between 85 bar and 5 bar. Furthermore, these materials had already been studied theoretically by Klontzas *et al.* with significant agreement between the experimental and theoretical analysis.<sup>81</sup> The authors also noted that the comparable H<sub>2</sub> uptake capacities of the group 3 COFs and MOFs in this study indicated that capacity is independent of the composition of the structure's backbone and is more correlated with the pore size of the framework. This phenomenon presents a physical limitation for these materials as COFs with large pore volumes are needed to obtain high H<sub>2</sub> uptake capacities, yet designing such a COF sacrifices the microporosity and strong adsorption sites that are prerequisites to increase gas uptake densities within these materials. This drawback was also evident from the gradual decrease in isosteric heats of adsorption (Q<sub>st</sub>) in group 3 COFs, which suggests the saturation of strong adsorption sites. This trend is characteristic of materials with high pore volumes because

low-pressure H<sub>2</sub> adsorption at 77 K is stronger in small pockets or corrugated surfaces relative to flat surfaces or edges.

Rather than sacrificing the high pore volume in COFs to achieve a higher density of strong binding sites, metal doping was proposed to introduce high-affinity sites and enhance H<sub>2</sub> storage performance at ambient temperatures. In 2009, Cao *et al.* calculated the hydrogen uptake of a series of Li-doped COFs compared to their undoped analogues.<sup>82</sup> In addition to stronger H<sub>2</sub> affinities, these simulations also revealed H<sub>2</sub> uptake for Li-doped COF-105 and COF-108 more than doubled relative to that of the pristine versions, reaching 6.84 and 6.73 wt %, respectively, at 298 K and 100 bar. The authors attributed the higher H<sub>2</sub> affinity to formation of a dative bond between the H<sub>2</sub> and the Li atom. A similar strategy has been extended to other 3D-COFs that contain anchored lithium alkoxide groups,<sup>83</sup> and substitutional doping<sup>84</sup> has been proposed and explored computationally. Finally, while experimental and computational results suggest COFs as potential materials for hydrogen storage, the practical implementation of COFs has yet to be realized.

### ***Porous Organic Polymers***

Amorphous porous organic polymers (POPs) have also been explored as potential candidates for hydrogen storage due to their ease of processibility and good mechanical stability. POPs are further divided into four groups: (1) hypercrosslinked polymers (HCPs), (2) conjugated microporous polymers (CMPs), (3) porous aromatic frameworks (PAFs), and (4) polymers of intrinsic microporosity (PIMs).

HCPs are co-polymers synthesized *via* Friedel–Crafts reactions that lead to the formation of very fine pore structures suitable for hydrogen storage applications. For example, poly(styrene-co-vinylbenzyl chloride) (PS-VBC) exhibited a surface area of approximately 2000 m<sup>2</sup> g<sup>-1</sup> with a hydrogen storage capacity of 5 wt % (77 K, 80 bar).<sup>85</sup> CMPs are 3D amorphous porous polymers constructed from rigid blocks and connected through  $\pi$ -conjugated bonds. Notable examples include HCMP-1<sup>86</sup> and POP-1<sup>87</sup>, which demonstrate moderate H<sub>2</sub> capacities of 0.95 wt % (77 K, 1.13 bar) and 2.78 wt % (77 K, 60 bar), respectively. No significant improvement has yet to be shown among other CMPs.<sup>88,89</sup>

In 2009, Ben *et al.* synthesized the porous aromatic framework PAF-1 constructed from tetrahedral tetraphenylene methane building units, which showed a high BET surface area of

5600 m<sup>2</sup> g<sup>-1</sup>. PAF-1 exhibits good thermal and hydrothermal stabilities owing to its diamond-like structure, and hydrogen isotherms at 77 K for PAF-1 demonstrated very high excess hydrogen uptake of 7.0 wt% at 48 bar.<sup>90</sup> Following this study, Yuan *et al.* synthesized a series of PAF-1 analogues by exchanging the central carbon atom of the tetrahedral monomers with adamantane (PPN-3), silicon (PPN-4), and germanium (PPN-5) and demonstrated a higher BET area for PPN-4 (6461 m<sup>2</sup> g<sup>-1</sup>) compared to PAF-1, along with a higher excess hydrogen uptake of 8.34 wt% (77 K, 55 bar).<sup>91</sup> The isosteric heats of adsorption for H<sub>2</sub> were 4 kJ mol<sup>-1</sup> and 4.6 kJ mol<sup>-1</sup> for PPN-4 and PAF-1, respectively, which show similar weak physisorbed H<sub>2</sub> affinity, leading the authors to mainly attribute the higher H<sub>2</sub> uptake capacity to the higher surface area.

PIMs attain their porosity from the inefficient packing of monomers during crosslinking of rigid, non-linear linkers. Extensive studies were performed on PIM-1 towards hydrogen storage, which demonstrated a relatively high surface area of approximately 1000 m<sup>2</sup> g<sup>-1</sup> and a moderate H<sub>2</sub> uptake of 1.7 wt % (77 K, 10 bar).<sup>92,93</sup> In 2019, Rochat *et al.* assessed the aging process and long-term stability of PIM-1 for hydrogen storage and found that the surface area was mostly retained after 400 days with a slight loss in hydrogen capacity that decreased 2.60 wt % (77 K, 100 bar) on day 1 to 1.90 wt % (77 K, 100 bar) on day 400.<sup>93</sup> In 2018, Bera *et al.* synthesized a series of triptycene-based microporous polymers (TMPs), which are similar to PIMs in their rigid backbones yet contain flexible benzylic bonds, and found that TMP-3 outperformed other PIMs in terms of low-pressure hydrogen uptake (2.21 wt % at 77 K and 1 bar).<sup>94</sup>

### *Carbon-based Materials*

Carbon-based materials, including porous carbons, carbon nanotubes, fibers, and fullerenes, have also been proposed as suitable sorbents for gas storage owing to their structural diversity. As a result, the porosity and structural composition of these materials can be tailored towards H<sub>2</sub> storage. Furthermore, the abundance, ease of processibility, ultra-light materials, and high chemical and thermal stability have also drawn great interest to investigations on carbon-based materials as H<sub>2</sub> sorbents.<sup>95</sup> This great interest paved the way to advances in the field during the late 1990s and early 2000s but plateaued soon after as it seemed an upper limit had been reached after the development of super-activated, porous carbons with large surface areas.<sup>96</sup> Activated carbons were first proposed due to their low cost, but typically form a large amount of

mesopores along with broad pore size distributions.<sup>95</sup> In contrast, super-activated carbons possess higher surface areas and more uniform pore size distributions.<sup>97</sup>

Another approach to synthesize high surface area carbon-based materials with uniform, ordered structures is through nano-casting onto a sacrificial template, such as silica,<sup>98</sup> zeolites,<sup>99</sup> aluminosilicates,<sup>99</sup> and MOFs.<sup>100</sup> From this, new classes of carbon-based materials emerged, including ordered mesoporous carbons (OMCs)<sup>101-103</sup> and zeolite-templated carbons (ZTCs)<sup>104-106</sup> that are synthesized from nano-casting onto mesoporous silica and zeolite templates, respectively. Lu *et al.* reported the first experimental results of hydrogen storage in a templated nanocarbon OMC, which exhibits a surface area of approximately 2310 m<sup>2</sup> g<sup>-1</sup> and hydrogen capacity of 1.78 wt % at 77 K and 1 bar.<sup>107</sup> In 2015, Gadiou *et al.* examined a series of OMCs, as well as previously published data towards hydrogen storage, and concluded that hydrogen storage at 77 K heavily relies on the presence of micropores as opposed to mesopores.<sup>108</sup> This was further confirmed in later studies that increased the amount micropores in OMCs to achieve higher hydrogen capacities.<sup>109-111</sup> The importance of micropores toward hydrogen storage was also evident in ZTCs, which are purely microporous materials. Notably, Yang *et al.* demonstrated this using a ZTC structure with H<sub>2</sub> uptake of 5.7 wt % at 77 K and 10 bar.<sup>112</sup>

Other efforts towards improving hydrogen capability in carbon-based materials include introduction of heteroatomic species such as nitrogen or boron, as well as other functional groups onto the framework.<sup>113,114</sup> In 2017, Blankenship *et al.* synthesized an oxygen-rich microporous carbon derived from cellulose acetate with high surface area of approximately 3800 m<sup>2</sup> g<sup>-1</sup> and gravimetric hydrogen excess uptake of 7.0% at 77K and 20 bar.<sup>115</sup> The authors also calculated the isosteric heat of adsorption to be 10 kJ mol<sup>-1</sup>, suggesting strong physisorption for this material. Finally, metal doping has also been shown to improve storage capability by providing stronger binding sites within the framework for hydrogen adsorption.<sup>116</sup>

In addition to synthesized carbon-based materials, commercially available carbon-based materials were also explored for hydrogen adsorption for comparison when studying other classes of materials. For example, Yaghi and coauthors reported the hydrogen adsorption performance of BPL carbon with a BET area of 1250 m<sup>2</sup> g<sup>-1</sup>.<sup>80</sup> At 77 K and 85 bar, BPL carbon displays a total hydrogen uptake of 3.9 wt % and a volumetric uptake of 35.6 g L<sup>-1</sup> considering

the bulk density of  $0.87 \text{ g cm}^{-3}$ . At 77 K, the 5-85 bar deliverable capacity of BPL carbon is 1.86 wt % ( $16.5 \text{ g L}^{-1}$ ).

### *Zeolites*

Zeolites are microporous adsorbents constructed from aluminosilicate materials with well-defined structure and accessible pores. Zeolites typically contain counterions that could affect the binding energies and interactions of guest molecules. Nonetheless, the binding energies of  $\text{H}_2$  in silica are generally quite similar to those of carbon.<sup>23</sup> Furthermore, zeolites are constructed from relatively heavier elements and typically contain lower void fractions, which hinders their implementation as hydrogen sorbents. As a result, limited research has been done regarding zeolites for hydrogen storage. In one notable example from 2003, Langmi *et al.* investigated the use of zeolites A, X, Y, and RHO to include a wide range of different compositions and pore geometries. Hydrogen capacities at 77 K and 15 bar were shown to be the higher for NaX, NaY, and MgY with 1.79, 1.81, and 1.74 wt %, respectively.<sup>76</sup> Other reports of FAU-type zeolites have also shown relatively low volumetric hydrogen uptake and delivery at 77 K and 298 K compared to other porous materials.<sup>23,117</sup>

## **4. Confinement of Hydrides of light elements in porous materials.**

### *Overview of HLEs and Initial Studies in Nanoconfinement*

Hydrides of light elements (HLEs), which are molecules that store hydrogen in the form of chemical bonds, hold great promise for on-board storage applications due to their extremely high gravimetric and volumetric densities, especially in the case of B-, N-, and C-based hydrides. Owing to the rich diversity in potential structures that can form between H and B, N, or C, the nature of the hydrogen species can range from hydridic to protonic depending on the identity of the bonding partner. HLEs can be broken down into four classes (**Figure 6**): 1) simple HLEs (e.g.,  $\text{NH}_3$ ,  $\text{B}_2\text{H}_6$ ,  $\text{NH}_3\text{-BH}_3$ ); 2) metalated HLEs (e.g.,  $\text{LiBH}_4$ ,  $\text{Mg}(\text{BH}_4)_2$ ); 3) composites ( $2\text{LiBH}_4\text{-MgH}_2$ ); and 4) complexes ( $\text{Mg}(\text{BH}_4)_2\cdot 2\text{NH}_3$ ). While each class of HLEs offers various advantages and drawbacks, in addition to featuring unique strategies to tune dehydrogenation thermodynamics, these topics have been reviewed in depth elsewhere, so we refer the reader there for further discussion.<sup>8</sup> As a class of materials, HLEs are typically limited in practical

applications by slow kinetics, irreversible H<sub>2</sub> loss, high temperatures required for H<sub>2</sub> desorption (reaching up to 350 °C in some cases), or the formation of unwanted by-products during operation (e.g., B<sub>2</sub>H<sub>6</sub> upon dehydrogenation of LiBH<sub>4</sub>). Researchers have investigated strategies to address these challenges and improve the performance of HLEs, and nanoconfinement of HLEs within porous materials has emerged as one of the most promising strategies, especially in the context of overcoming kinetic limitations. For example, both insufficient contact between reacting species and the relatively large particle sizes of HLEs limit the kinetic release of H<sub>2</sub>, and aggregation of HLE particles upon cycling further compounds this problem (**Figure 6**).<sup>8</sup> Confinement of the HLE particles within a porous framework can resolve both limitations, while also decreasing mass diffusion pathways and improving contact between reactants, ultimately affording a significant improvement in kinetic H<sub>2</sub> desorption properties.

In 2005, Gutowska *et al.* reported that confinement of NH<sub>3</sub>–BH<sub>3</sub> in the silica-based framework SBA-15, which contains nanoporous 1-D channels, led to a significant improvement in ammonia–borane dehydrogenation properties, and this early success stimulated subsequent investigations into HLE nanoconfinement.<sup>118</sup> Since then, researchers have expanded studies with SBA-15 to include other classes of HLEs, such as LiBH<sub>4</sub><sup>119,120</sup> and NaZn(BH<sub>4</sub>)<sub>3</sub><sup>121</sup>, with promising results, while also exploring complementary strategies to improve performance, such as the incorporation of transition metal nanoparticles<sup>122</sup> within the nanoporous channels of SBA-15. As the materials community searched for more sophisticated materials to improve HLE confinement properties, exciting developments in emerging classes of porous materials offered new avenues for exploration. As a result, studies on HLE nanoconfinement have expanded to include a wider range of porous materials, particularly porous carbons, metal–organic frameworks, and zeolites, with exciting results that may soon result in practical applications that leverage HLEs.

### *HLEs in Mesoporous Carbons*

Carbon-based materials are perhaps the most widely used nanoscale host materials for HLE confinement as they are extremely lightweight, which minimizes the energy density penalty that results from the dead-weight of the host material, and they are thermally stable under conditions required for reversible H<sub>2</sub> release.<sup>123</sup> Additionally, researchers have reported

straightforward strategies to access mesoporous carbon scaffolds with narrow pore size distributions from polymer-based precursors;<sup>124,125</sup> these scaffolds improve hydrogen desorption performance of LiBH<sub>4</sub> by significantly decreasing the onset desorption performance and eliminating the formation of unwanted diborane (B<sub>2</sub>H<sub>6</sub>) by-products during this process. The identity of the carbon host can also influence performance, as evidenced by the incorporation of graphene into the mesoporous host using a graphene hydrogel precursor that results in improved LiBH<sub>4</sub> loadings.<sup>126</sup> Alternatively, doping a mesoporous carbon framework with nitrogen presents a strategy to access reversible H<sub>2</sub> release from LiAlH<sub>4</sub> *via* enhanced host-guest interactions between the carbon scaffold and the HLE particles.<sup>123</sup> As a complement to extended carbon framework structures, hollow carbon nanospheres (HCNs) also show promise as mesoporous adsorbents for nanoconfinement of borohydride-based HLEs.<sup>127-130</sup> HCNs are potentially advantageous compared to extended porous scaffolds as the host material dead-weight is minimized, and the thin porous HCN shell may be relatively easier for HLEs to infiltrate.<sup>130</sup>

Although confinement of HLEs in porous materials presents a viable strategy to significantly reduce hydrogen desorption temperatures by at least 100 °C compared to those of their bulk hydrides (e.g., 400 °C for bulk LiBH<sub>4</sub><sup>131</sup> to temperatures as low as 150 °C for LiBH<sub>4</sub>/SBA-15<sup>119</sup>), these desorption temperatures are still high for practical implementation in on-board storage systems. One promising approach to further decrease the onset temperature involves the incorporation of catalytic metal nanoparticles (NPs) within the mesoporous carbon frameworks, offering access to systems that release hydrogen reversibly at room temperature. One of the most straightforward strategies to incorporate metal NPs into porous carbon scaffolds includes the *in situ* generation of NPs within the scaffold starting from metal salt precursors.<sup>132-135</sup> Notably, this method offers access to metal NPs with tunable sizes that vary based on the pore structure of the carbon scaffold, and alloys are easily attainable by using additional metal salt precursors during synthesis. Alternatively, researchers have demonstrated that using MOFs or ZIFs as templates enables access to well-defined, hierarchically porous carbon scaffolds upon pyrolysis that contain evenly dispersed metal nanoparticles throughout the host material. Importantly, this strategy affords NPs encapsulated by the porous carbon shell (i.e., NP@Carbon architectures) that can both limit aggregation and prevent leaching of the metal NPs, while also ensuring close contact between the NP catalyst and HLE upon incorporation of the HLE within the porous carbon shell. Finally, mesoporous carbon-supported NP composites are also

accessible without the use of porous templates as precursors, further exemplifying the large synthetic diversity available to porous carbon scaffolds used for HLE confinement.<sup>136,137</sup>

### *HLEs in Metal Oxides and Aluminosilicate Clays*

To access more chemically diverse scaffolds, researchers shifted to other porous hosts, such as metal oxides and aluminosilicate clays, to alter the reactivity of the encapsulated HLE beyond just preventing agglomeration. In one example, Liu *et al.* confined LiBH<sub>4</sub> inside TiO<sub>2</sub> microtubes through a chemical impregnation approach and investigated increasing equivalences of TiO<sub>2</sub> on the LiBH<sub>4</sub> reactivity.<sup>138</sup> The LiBH<sub>4</sub>@TiO<sub>2</sub> (26 wt % LiBH<sub>4</sub>) composite exhibited a peak H<sub>2</sub> desorption temperature at 183 °C, while decreasing LiBH<sub>4</sub> loadings 14 wt % resulted in a release temperature of 100 °C. Importantly, these temperatures are well below that observed for bulk LiBH<sub>4</sub> (445 °C). Powder X-ray diffraction (PXRD) analysis of post-hydrogenated materials illustrated the formation of LiTiO<sub>2</sub> in the composite, suggesting a redox reaction during the dehydrogenation process. The  $E_a$  of dehydrogenation decreased by over 20 kJ mol<sup>-1</sup> in the LiBH<sub>4</sub> composite as compared to bulk LiBH<sub>4</sub>, which the authors attributed to the confinement of the HLE in addition to a destabilizing effect imparted by the non-innocent TiO<sub>2</sub> support. Beyond encapsulating HLEs into existing supports *via* solvent impregnation, atomic layer deposition was explored by Leick *et al.* to coat porous  $\gamma$ -Mg(BH<sub>4</sub>)<sub>2</sub> with Al<sub>2</sub>O<sub>3</sub> as an outer shell support.<sup>139</sup> While the coating failed to prevent the HLE from heat-induced agglomeration during the dehydrogenation process, the interesting proof of concept composite doubled the low-temperature H<sub>2</sub> capacity, increased the dehydrogenation kinetics by a factor of 3, and prevented the release of diborane as a side product in comparison to  $\gamma$ -Mg(BH<sub>4</sub>)<sub>2</sub>. Thus, this study motivates the further development of Al-based scaffolds to encapsulate HLEs yet highlights the importance of more rigid pores within a HLE composite to prevent particle agglomeration. Some porous scaffolds offer favorable pendant linkers that can interact with HLEs. With this strategy in hand, Zhang and co-workers explored the encapsulation of ammonia borane (AB) in Pd-decorated halloysite nanotubes (Al<sub>2</sub>Si<sub>2</sub>O<sub>5</sub>(OH)<sub>4</sub>·nH<sub>2</sub>O; HNT) given the abundant hydroxyl groups present in the natural clay.<sup>140</sup> The Pd-doped HNT support facilitated the dehydrogenation of AB while also preventing the formation of volatile impurities like ammonia, diborane, and borazine. The authors attributed these phenomena to hydroxyls from the HNT forming interfacial

coordination bonds with  $\text{-BH}_3$  on AB and Pd interacting with  $\text{-NH}_3$  on AB, thus weakening the B-H and N-H bonds as observed in Fourier transformed infrared spectroscopic (FTIR) experiments.

### *HLEs Encapsulated within Metal–Organic Frameworks*

While the previously mentioned porous materials offer favorable confinement effects to stabilize HLEs, the pore sizes are often heterogeneous and lack structural handles for precise tuning.<sup>8,141</sup> In contrast, hybrid porous materials known as MOFs feature pores that are well-defined by the self-assembly of inorganic nodes and multitopic organic linkers. In addition to offering adsorptive sites for the selective storage and delivery of  $\text{H}_2$ , as discussed in previous sections, MOF pores can also serve as supports for the immobilization of hydrogen-rich guests, such as HLEs. In this section, we will highlight recent studies that chronicle the effects of MOF pore functionalization on anchored HLEs and the corresponding hydrogen storage and delivery properties.

Early work demonstrated the incorporation of HLEs within MOF pores, yet the HLEs persisted as nanoclusters limited by only the MOF pore size.<sup>142-148</sup> Thus, the challenge remained to anchor one HLE to a MOF support without further agglomeration. Allendorf, Stavila, and teams investigated the confinement of  $\text{Mg}(\text{BH}_4)_2$  within UiO-67-bpy, a MOF consisting of  $\text{Zr}_6\text{O}_8$  nodes and 2,2'-bipyridine-5,5'-dicarboxylate ( $\text{bpydc}^{2-}$ ) linkers.<sup>24</sup> The authors selected the  $\text{bpydc}^{2-}$  linkers to utilize the N atoms (1) to anchor discrete molecules of  $\text{Mg}(\text{BH}_4)_2$  and (2) to affect the hydrogen release pathway, as demonstrated from prior work in porous carbons.<sup>149,150</sup> Solvent impregnation of  $\text{Mg}(\text{BH}_4)_2$  inside UiO-67-bpy formed  $\text{Mg}(\text{BH}_4)_2@ \text{UiO-67bpy}$ , with Mg coordinated to the N on the bpy linker as determined through IR and X-ray adsorption spectroscopy and complemented through DFT calculations. Thermogravimetric analysis (TGA) demonstrated a  $\text{H}_2$  desorption onset temperature at 120 °C in  $\text{Mg}(\text{BH}_4)_2@ \text{UiO-67bpy}$ , which is ~150 °C lower than the desorption temperature observed in  $\text{Mg}(\text{BH}_4)_2$ . Residual gas analyzer-based mass spectrometry (RGA-MS) confirmed the identity of released  $\text{H}_2$ , as opposed to undesired boron-containing species like  $[\text{B}_{12}\text{H}_{12}]^{2-}$  and  $[\text{B}_{10}\text{H}_{10}]^{2-}$ , from  $\text{Mg}(\text{BH}_4)_2@ \text{UiO-67-bpy}$  at low temperatures. Thus, the favorable nanoconfinement of the HLE in the MOF pore (~1 nm) likely precluded the formation of such bulkier species. However, despite the lower  $\text{H}_2$  desorption

temperature, the HLE/MOF composite only released 0.22 wt % H<sub>2</sub> at 150 °C or 1 wt % H<sub>2</sub> when normalized to Mg(BH<sub>4</sub>)<sub>2</sub>. Moreover, <sup>11</sup>B variable temperature NMR spectroscopic studies suggested the formation of additional stable B-O species at the MOF node, which could account for the poor H<sub>2</sub> desorption. Furthermore, the composite displayed a decrease in the long-range order after dehydrogenation from weak intensity observed in PXRD patterns and the absence of MOF-hydride IR signals. Attempts to rehydrogenate the composite were unsuccessful given the higher hydrogen pressures and temperatures required for Mg(BH<sub>4</sub>)<sub>2</sub>, which are beyond the limits of the parent host UiO-67-bpy. Modeling calculations indicated that the low H<sub>2</sub> desorption temperature is favored by chelation of the Mg(BH<sub>4</sub>)<sub>2</sub> to the O and N sites on the MOF. Ultimately, this study demonstrated a pivotal design strategy to target molecular dispersion of an HLE within a porous host, possible only with the tunability and long-range order that MOFs offer.

In addition to the MOF linker, the MOF node can help anchor nanoconfined HLE species. To this end, Zou and co-workers impregnated MgH<sub>2</sub> onto a Ni-based MOF composed of trimesic acid linkers to encapsulate 3 nm MgH<sub>2</sub> nanocrystals.<sup>151</sup> However, they observed that the Ni nodes reacted with the edges of the MgH<sub>2</sub> nanocrystals to form Mg<sub>2</sub>Ni/ Mg<sub>2</sub>NiH<sub>4</sub> sites on the outer shell of the nanocrystals through high-resolution transmission electron microscopy (HRTEM) and PXRD. Following the formation of the composite, the respective hydrogen uptake and release enthalpies were  $-65.7 \pm 2.1$  and  $69.7 \pm 2.7$  kJ mol<sup>-1</sup> H<sub>2</sub>, lower than those reported of bulk MgH<sub>2</sub>.<sup>152</sup> Moreover, the Mg@Ni-MOF composite demonstrated rapid adsorption of H<sub>2</sub>, uptaking 1 wt % H<sub>2</sub> within the first 110 s at 673 K and 623 K, which were comparable to that of MgH<sub>2</sub>. MgH<sub>2</sub>@Ni-MOF desorbed 1.5 wt % and 0.52 wt % H<sub>2</sub> in 150 s at 623 K and 473 K, while MgH<sub>2</sub> released 0.42 and 0.16 wt % in 2 hours at 548 and 498 K, respectively. The authors attribute the improved H<sub>2</sub> storage and release properties to the nanoconfinement of MgH<sub>2</sub>, the aggregation prevention offered by the Ni-MOF, and the dissolution of H<sub>2</sub> into H atoms facilitated by the Mg<sub>2</sub>Ni outershell.

Beyond serving as anchoring sites for HLEs, MOF structural elements can influence the hydrogen storage kinetics of encapsulated HLE clusters. For example, Peil *et al.* investigated the H<sub>2</sub> release from ammonia borane (AB) confined within a family of MIL-53 MOFs varying in linker functionality and metal node identity.<sup>153</sup> First, the authors probed the effect of functionalized terephthalic acids (e.g., 2-hydroxyterephthalic acid and 2-aminoterephthalic acid)

following the favorable effect of N and O sites observed in the aforementioned  $\text{Mg}(\text{BH}_4)_2@ \text{UiO}-67\text{-bpy}$  study.<sup>24</sup> The amino and hydroxy functionalized linkers in Al-MIL-53-NH<sub>2</sub> and Al-MIL-53-OH, respectively, achieved H<sub>2</sub> evolution < 100 °C, surpassing that of bulk AB at 100 °C, yet only achieved a normalized H<sub>2</sub> release of 67% and 38%, respectively, in comparison to the 100% achieved by bulk ammonia borane. The AB encapsulated in unfunctionalized Al-MIL-53 released H<sub>2</sub> at ~150 °C, yet desorbed 86% H<sub>2</sub> from the encapsulated ammonia borane. Interestingly, the amino and hydroxy substituents likely caused a structural change in the confined AB as determined by a change in the <sup>11</sup>B NMR of the bulk HLE with the encapsulated HLE. Next, the authors studied the combination of terephthalic acid with Al, Cr, Fe, and V nodes to form MIL-53 or structurally similar MIL-47. Fe-MIL-53 exhibited rapid H<sub>2</sub> release around 100 °C, greater than that of Al-MIL-53, V-MIL-47, Cr-MIL-53, and bulk AB. AB in Fe-MIL-53 released 226% of H<sub>2</sub> as normalized to the corresponding wt % of bulk AB, suggesting a partial decomposition of the Fe-MIL-53 framework to liberate the detected H<sub>2</sub>. Such an unexpected decomposition route was also suggested through a lower crystallinity PXRD pattern of Fe-MIL-53 after dehydrogenation. As compared to bulk AB, the other MOF nodes (Al, V, Cr) neither reduced the H<sub>2</sub> desorption temperature nor improve the H<sub>2</sub> release percentages, suggesting that modifying MOF linkers is a more efficacious route for imparting nanoconfinement effects in MOF HLE hosts. In summary, the tunability that MOF scaffolds offer remains unparalleled, while the uniform pore environments can engender consistent sizes, and subsequently unique reactivity patterns, of the encapsulated HLE that allows for more informed material design. However, the practical incorporation of MOF-based HLE composites in hydrogen delivery settings is challenged by the excess weight of the heavy metal-oxo based scaffolds, as well as the thermal sensitivity of most frameworks.

## 5. Outlook

Despite efforts in developing solid-state porous materials for hydrogen storage applications, the gap between the performance of current storage materials and the need for high-performing storage system capable of meeting the DOE requirements at near room temperature remains a grand challenge in the hydrogen storage economy. In this regard, we offer an outlook on the future implementation of hydrogen storage materials in hydrogen-powered fuel cell

automobiles from three aspects, including chemistry and material science, engineering, and commercialization. We hope to encourage both fundamental and applied research in the field of solid-state porous materials for hydrogen storage, which will be necessary to realize hydrogen as a viable energy source for transportation. If widely adopted on large scales, this clean energy platform could enable the introduction of carbon-neutral energy systems capable of mitigating both energy and environmental problems facing our world today.

### ***5.1 Chemistry and material science***

Researchers will continue to seek to leverage synthetic and computational tools to design better porous materials for hydrogen storage that exhibit large, balanced volumetric and gravimetric capacities at ambient temperatures. To achieve this objective, new high-throughput methodologies, which consist of both state-of-art simulation and automated synthesis, can be applied to direct the precise synthesis of high-performing hydrogen storage materials. Further enhancing hydrogen storage performance at ambient temperatures might require a higher density of accessible, low-valent metal sites, or the incorporation of moieties with higher affinities to hydrogen within respective porous materials to increase the strength of hydrogen–framework interactions, all while maintaining the optimal porosities and surface areas of the parent frameworks. In addition, clear fundamental understandings of both the kinetics and thermodynamics during hydrogen adsorption and desorption processes could offer insight on achieving fast adsorption-desorption cycling with high storage capacities.

### ***5.2 Engineering***

System-level hydrogen capacities are more relevant than material-level values in term of practical performance. The calculation of volumetric capacity for crystalline materials like MOFs is often based on the crystallographic density. The actual packing density is generally lower than ideal crystallographic density because of the inherent mechanical stability of materials and packing-related voids. Thus, it is important to develop shaping techniques using tools such as 3-D printing, high-pressure compaction, or the addition of chemical binders to integrate high-performing adsorbent powders into viable adsorptive pellets, eventually enhancing the packing efficiency. Specifically, researchers should consider the balance of processability, mechanical stability, and gas adsorption performance. In addition, the thermal management of pressed pellets of porous materials is another vital factor that influences refueling time. For example, strategies

to improve the thermal conductivity of adsorbents, such as high-performing MOF materials, can dissipate the heat generated during adsorption, thus decreasing refueling time of hydrogen. Since the storage system is expected to last over the entire life of hydrogen-powered vehicles, researchers should investigate the chemical, hydrolytic, thermal, and mechanical stability of the pressed pellets to achieve long-term utility for on-board hydrogen storage.

### **5.3 Commercialization**

Once a high-performance hydrogen adsorbent and related adsorptive system are fully developed, the next step involves the scale-up and commercialization of this technology. In this regard, environmentally friendly, inexpensive, and safe synthetic approaches are favorable for the large-scale manufacturing of porous materials; in particular, electrosynthesis, mechanochemical synthesis, and water-based synthesis of porous materials offer attractive and potentially scalable routes.<sup>154-156</sup> Moreover, some startup companies have already begun commercializing MOFs by employing large-scale syntheses with cost-saving solvent recycling systems. In addition, techno-economic analysis is important consideration when developing porous materials for practical implementation.<sup>157</sup> Ideally, in the case of MOF production, researchers can take advantage of precise self-assembly strategies to select metal salts and ligands with reasonable prices for the synthesis of targeted porous material candidates with reduced cost. Ultimately, solid-state porous materials are poised for realization of next-generation hydrogen storage systems capable of large-scale commercialization and implementation.

### **ACKNOWLEDGMENTS**

The authors gratefully acknowledge support from the U. S. Department of Energy's Office of Energy Efficiency and Renewable Energy(EERE) under award no. DE-EE0008816. K.O.K. gratefully acknowledges support from the IIN Postdoctoral Fellowship and the Northwestern University International Institute for Nanotechnology. M.C.W. is supported by the NSF Graduate Research Fellowship under grant DGE-1842165.

### **AUTHOR CONTRIBUTIONS**

Z.C. and O.K.F. proposed the topic of the manuscript. All authors were involved in the writing of the manuscript and approved the final version of the manuscript.

## Declaration of Interests

O.K.F. has a financial interest in NuMat Technologies, a startup company that is seeking to commercialize MOFs.

## References

1. BP. BP Statistical Review of World Energy. <http://bp.com/statisticalreview> (BP, 2019).
2. Chu, S., and Majumdar, A. (2012). Opportunities and challenges for a sustainable energy future. *Nature* *488*, 294-303.
3. Trends in Atmospheric Carbon Dioxide, Global Monitoring Laboratory (GML) of the National Oceanic and Atmospheric Administration (NOAA), <https://gml.noaa.gov/ccgg/trends/global.html> (accessed June 20, 2021).
4. Lee, R. (2011). The Outlook for Population Growth. *Science* *333*, 569.
5. Jacobson, M.Z., Colella, W.G., and Golden, D.M. (2005). Cleaning the Air and Improving Health with Hydrogen Fuel-Cell Vehicles. *Science* *308*, 1901-1905.
6. Durbin, D.J., and Malardier-Jugroot, C. (2013). Review of hydrogen storage techniques for on board vehicle applications. *Int. J. Hydrogen Energy* *38*, 14595-14617.
7. Broom, D.P., Webb, C.J., Hurst, K.E., Parilla, P.A., Gennett, T., Brown, C.M., Zacharia, R., Tylianakis, E., Klontzas, E., Froudakis, G.E., et al. (2016). Outlook and challenges for hydrogen storage in nanoporous materials. *Appl. Phys. A* *122*, 151.
8. He, T., Pachfule, P., Wu, H., Xu, Q., and Chen, P. (2016). Hydrogen carriers. *Nat Rev Mater.* *1*, 16059.
9. Hydrogen Storage, Hydrogen and Fuel Cell Technologies Office, U.S. Department of Energy, <https://www.energy.gov/eere/fuelcells/hydrogen-storage>, accessed September 2021.
10. Ross, D.K. (2006). Hydrogen storage: The major technological barrier to the development of hydrogen fuel cell cars. *Vacuum* *80*, 1084-1089.
11. Allendorf, M.D., Hulvey, Z., Gennett, T., Ahmed, A., Autrey, T., Camp, J., Seon Cho, E., Furukawa, H., Haranczyk, M., Head-Gordon, M., et al. (2018). An assessment of strategies for the development of solid-state adsorbents for vehicular hydrogen storage. *Energy Environ. Sci.* *11*, 2784-2812.
12. Target Explanation Document: Onboard Hydrogen Storage for Light-Duty Fuel Cell Vehicles, U.S. Department of Energy, <https://www.energy.gov/eere/fuelcells/downloads/target-explanation-document-onboard-hydrogen-storage-light-duty-fuel-cell>, accessed May 2020.
13. Rosi, N.L., Eckert, J., Eddaoudi, M., Vodak, D.T., Kim, J., Keeffe, M., and Yaghi, O.M. (2003). Hydrogen Storage in Microporous Metal-Organic Frameworks. *Science* *300*, 1127-1129.
14. Murray, L.J., Dincă, M., and Long, J.R. (2009). Hydrogen storage in metal-organic frameworks. *Chem. Soc. Rev.* *38*, 1294-1314.
15. Sculley, J., Yuan, D., and Zhou, H.-C. (2011). The current status of hydrogen storage in metal-organic frameworks—updated. *Energy Environ. Sci.* *4*, 2721-2735.
16. Suh, M.P., Park, H.J., Prasad, T.K., and Lim, D.-W. (2012). Hydrogen Storage in Metal-Organic Frameworks. *Chem. Rev.* *112*, 782-835.

17. Côté, A.P., Benin, A.I., Ockwig, N.W., O'Keeffe, M., Matzger, A.J., and Yaghi, O.M. (2005). Porous, Crystalline, Covalent Organic Frameworks. *Science* *310*, 1166-1170.
18. Ding, S.-Y., and Wang, W. (2013). Covalent organic frameworks (COFs): from design to applications. *Chem. Soc. Rev.* *42*, 548-568.
19. Han, S.S., Furukawa, H., Yaghi, O.M., and Goddard, W.A. (2008). Covalent Organic Frameworks as Exceptional Hydrogen Storage Materials. *J. Am. Chem. Soc.* *130*, 11580-11581.
20. Xu, Y., Jin, S., Xu, H., Nagai, A., and Jiang, D. (2013). Conjugated microporous polymers: design, synthesis and application. *Chem. Soc. Rev.* *42*, 8012-8031.
21. Cousins, K., and Zhang, R. (2019). Highly Porous Organic Polymers for Hydrogen Fuel Storage. *Polymers* *11*.
22. Ströbel, R., Garche, J., Moseley, P.T., Jörissen, L., and Wolf, G. (2006). Hydrogen storage by carbon materials. *Journal of Power Sources* *159*, 781-801.
23. Lopes, F.V.S., Grande, C.A., Ribeiro, A.M., Loureiro, J.M., Evaggelos, O., Nikolakis, V., and Rodrigues, A.E. (2009). Adsorption of H<sub>2</sub>, CO<sub>2</sub>, CH<sub>4</sub>, CO, N<sub>2</sub> and H<sub>2</sub>O in Activated Carbon and Zeolite for Hydrogen Production. *Sep. Sci. Technol.* *44*, 1045-1073.
24. Schneemann, A., Wan, L.F., Lipton, A.S., Liu, Y.-S., Snider, J.L., Baker, A.A., Sugar, J.D., Spataru, C.D., Guo, J., Autrey, T.S., et al. (2020). Nanoconfinement of Molecular Magnesium Borohydride Captured in a Bipyridine-Functionalized Metal–Organic Framework. *ACS Nano* *14*, 10294-10304.
25. Kitagawa, S. (2017). Future Porous Materials. *Acc. Chem. Res.* *50*, 514-516.
26. Furukawa, H., Cordova, K.E., O'Keeffe, M., and Yaghi, O.M. (2013). The Chemistry and Applications of Metal–Organic Frameworks. *Science* *341*, 1230444.
27. Chen, Z., Li, P., Anderson, R., Wang, X., Zhang, X., Robison, L., Redfern, L.R., Moribe, S., Islamoglu, T., Gómez-Gualdrón, D.A., et al. (2020). Balancing volumetric and gravimetric uptake in highly porous materials for clean energy. *Science* *368*, 297-303.
28. Ahmed, A., Seth, S., Purewal, J., Wong-Foy, A.G., Veenstra, M., Matzger, A.J., and Siegel, D.J. (2019). Exceptional hydrogen storage achieved by screening nearly half a million metal-organic frameworks. *Nat. Commun.* *10*, 1568.
29. Denysenko, D., Grzywa, M., Jelic, J., Reuter, K., and Volkmer, D. (2014). Scorpionate-Type Coordination in MFU-4l Metal–Organic Frameworks: Small-Molecule Binding and Activation upon the Thermally Activated Formation of Open Metal Sites. *Angew. Chem. Int. Ed.* *53*, 5832-5836.
30. Jaramillo, D.E., Jiang, H.Z.H., Evans, H.A., Chakraborty, R., Furukawa, H., Brown, C.M., Head-Gordon, M., and Long, J.R. (2021). Ambient-Temperature Hydrogen Storage via Vanadium(II)-Dihydrogen Complexation in a Metal–Organic Framework. *J. Am. Chem. Soc.* *143*, 6248-6256.
31. Bucior, B.J., Bobbitt, N.S., Islamoglu, T., Goswami, S., Gopalan, A., Yildirim, T., Farha, O.K., Bagheri, N., and Snurr, R.Q. (2019). Energy-based descriptors to rapidly predict hydrogen storage in metal–organic frameworks. *Mol. Syst. Des. Eng.* *4*, 162-174.
32. García-Holley, P., Schweitzer, B., Islamoglu, T., Liu, Y., Lin, L., Rodriguez, S., Weston, M.H., Hupp, J.T., Gómez-Gualdrón, D.A., Yildirim, T., and Farha, O.K. (2018). Benchmark Study of Hydrogen Storage in Metal–Organic Frameworks under Temperature and Pressure Swing Conditions. *ACS Energy Lett.* *3*, 748-754.

33. Siegel, D. J., Hardy, B., HSECoE Team. Engineering an Adsorbent-Based Hydrogen Storage System: What Have We Learned? [https://www.energy.gov/sites/prod/files/2015/02/f19/fcto\\_h2\\_storage\\_summit\\_siegel.pdf](https://www.energy.gov/sites/prod/files/2015/02/f19/fcto_h2_storage_summit_siegel.pdf) (accessed Dec 2021).
34. Furukawa, H., Ko, N., Go, Y.B., Aratani, N., Choi, S.B., Choi, E., Yazaydin, A.Ö., Snurr, R.Q., O’Keeffe, M., Kim, J., and Yaghi, O.M. (2010). Ultrahigh Porosity in Metal–Organic Frameworks. *Science* 329, 424-428.
35. Furukawa, H., Miller, M.A., and Yaghi, O.M. (2007). Independent verification of the saturation hydrogen uptake in MOF-177 and establishment of a benchmark for hydrogen adsorption in metal–organic frameworks. *J. Mater. Chem.* 17, 3197-3204.
36. Eddaoudi, M., Moler, D.B., Li, H., Chen, B., Reineke, T.M., O’Keeffe, M., and Yaghi, O.M. (2001). Modular Chemistry: Secondary Building Units as a Basis for the Design of Highly Porous and Robust Metal–Organic Carboxylate Frameworks. *Acc. Chem. Res.* 34, 319-330.
37. Yaghi, O.M., O’Keeffe, M., Ockwig, N.W., Chae, H.K., Eddaoudi, M., and Kim, J. (2003). Reticular synthesis and the design of new materials. *Nature* 423, 705-714.
38. Ockwig, N.W., Delgado-Friedrichs, O., O’Keeffe, M., and Yaghi, O.M. (2005). Reticular Chemistry: Occurrence and Taxonomy of Nets and Grammar for the Design of Frameworks. *Acc. Chem. Res.* 38, 176-182.
39. Delgado-Friedrichs, O., O’Keeffe, M., and Yaghi, O.M. (2007). Taxonomy of periodic nets and the design of materials. *Phys. Chem. Chem. Phys.* 9, 1035-1043.
40. Yaghi, O.M., Kalmutzki, M.J., and Diercks, C.S. (2019). Introduction to Reticular Chemistry: Metal–Organic Frameworks and Covalent Organic Frameworks (John Wiley & Sons).
41. Cadiau, A., Adil, K., Bhatt, P.M., Belmabkhout, Y., and Eddaoudi, M. (2016). A metal–organic framework–based splitter for separating propylene from propane. *Science* 353, 137-140.
42. Cui, X., Chen, K., Xing, H., Yang, Q., Krishna, R., Bao, Z., Wu, H., Zhou, W., Dong, X., Han, Y., et al. (2016). Pore chemistry and size control in hybrid porous materials for acetylene capture from ethylene. *Science* 353, 141-144.
43. Li, B., Wen, H.-M., Zhou, W., Xu, Jeff Q., and Chen, B. (2016). Porous Metal–Organic Frameworks: Promising Materials for Methane Storage. *Chem* 1, 557-580.
44. Farha, O.K., Yazaydin, A.O., Eryazici, I., Malliakas, C.D., Hauser, B.G., Kanatzidis, M.G., Nguyen, S.T., Snurr, R.Q., and Hupp, J.T. (2010). De novo synthesis of a metal–organic framework material featuring ultrahigh surface area and gas storage capacities. *Nat. Chem.* 2, 944-948.
45. Nouar, F., Eubank, J.F., Bousquet, T., Wojtas, L., Zaworotko, M.J., and Eddaoudi, M. (2008). Supermolecular Building Blocks (SBBs) for the Design and Synthesis of Highly Porous Metal–Organic Frameworks. *J. Am. Chem. Soc.* 130, 1833-1835.
46. Eubank, J.F., Nouar, F., Luebke, R., Cairns, A.J., Wojtas, Ł., Alkordi, M., Bousquet, T., Hight, M.R., Eckert, J., Embs, J.P., et al. (2012). On Demand: The Singular rht Net, an Ideal Blueprint for the Construction of a Metal–Organic Framework (MOF) Platform. *Angew. Chem. Int. Ed.* 51, 10099-10103.
47. Luebke, R., Weseliński, Ł.J., Belmabkhout, Y., Chen, Z., Wojtas, Ł., and Eddaoudi, M. (2014). Microporous Heptazine Functionalized (3,24)-Connected rht-Metal–Organic

- Framework: Synthesis, Structure, and Gas Sorption Analysis. *Cryst. Growth Des.* *14*, 414-418.
48. Wilmer, C.E., Leaf, M., Lee, C.Y., Farha, O.K., Hauser, B.G., Hupp, J.T., and Snurr, R.Q. (2012). Large-scale screening of hypothetical metal–organic frameworks. *Nat. Chem.* *4*, 83-89.
  49. Colón, Y.J., Fairen-Jimenez, D., Wilmer, C.E., and Snurr, R.Q. (2014). High-Throughput Screening of Porous Crystalline Materials for Hydrogen Storage Capacity near Room Temperature. *J. Phys. Chem. C* *118*, 5383-5389.
  50. Colón, Y.J., and Snurr, R.Q. (2014). High-throughput computational screening of metal–organic frameworks. *Chem. Soc. Rev.* *43*, 5735-5749.
  51. Ahmed, A., Liu, Y., Purewal, J., Tran, L.D., Wong-Foy, A.G., Veenstra, M., Matzger, A.J., and Siegel, D.J. (2017). Balancing gravimetric and volumetric hydrogen density in MOFs. *Energy Environ. Sci.* *10*, 2459-2471.
  52. Feng, D., Chung, W.-C., Wei, Z., Gu, Z.-Y., Jiang, H.-L., Chen, Y.-P., Darensbourg, D.J., and Zhou, H.-C. (2013). Construction of Ultrastable Porphyrin Zr Metal–Organic Frameworks through Linker Elimination. *J. Am. Chem. Soc.* *135*, 17105-17110.
  53. Gomez-Gualdrón, D.A., Colon, Y.J., Zhang, X., Wang, T.C., Chen, Y.-S., Hupp, J.T., Yildirim, T., Farha, O.K., Zhang, J., and Snurr, R.Q. (2016). Evaluating topologically diverse metal-organic frameworks for cryo-adsorbed hydrogen storage. *Energy Environ. Sci.* *9*, 3279-3289.
  54. Gómez-Gualdrón, D.A., Wang, T.C., García-Holley, P., Sawelewa, R.M., Argueta, E., Snurr, R.Q., Hupp, J.T., Yildirim, T., and Farha, O.K. (2017). Understanding Volumetric and Gravimetric Hydrogen Adsorption Trade-off in Metal–Organic Frameworks. *ACS Appl. Mater. Interfaces* *9*, 33419-33428.
  55. Zhang, X., Lin, R.-B., Wang, J., Wang, B., Liang, B., Yildirim, T., Zhang, J., Zhou, W., and Chen, B. (2020). Optimization of the Pore Structures of MOFs for Record High Hydrogen Volumetric Working Capacity. *Adv. Mater.* *32*, 1907995.
  56. Chen, Z., Mian, M.R., Lee, S.-J., Chen, H., Zhang, X., Kirlikovali, K.O., Shulda, S., Melix, P., Rosen, A.S., Parilla, P.A., et al. (2021). Fine-Tuning a Robust Metal–Organic Framework toward Enhanced Clean Energy Gas Storage. *J. Am. Chem. Soc.* *143*, 18838-18843.
  57. Chen, Z., Li, P., Zhang, X., Li, P., Wasson, M.C., Islamoglu, T., Stoddart, J.F., and Farha, O.K. (2019). Reticular Access to Highly Porous acs-MOFs with Rigid Trigonal Prismatic Linkers for Water Sorption. *J. Am. Chem. Soc.* *141*, 2900-2905.
  58. Rouquerol, J.L., P.; Rouquerol, F. (2007). In *Studies in Surface Science and Catalysis*. In P.L.R.-R. Llewellyn, F.; Rouquerol, J.; Seaton, N., Eds, ed. (Elsevier), pp. 49.
  59. Gómez-Gualdrón, D.A., Moghadam, P.Z., Hupp, J.T., Farha, O.K., and Snurr, R.Q. (2016). Application of Consistency Criteria To Calculate BET Areas of Micro- And Mesoporous Metal–Organic Frameworks. *J. Am. Chem. Soc.* *138*, 215-224.
  60. Bhatia, S.K., and Myers, A.L. (2006). Optimum Conditions for Adsorptive Storage. *Langmuir* *22*, 1688-1700.
  61. Target Explanation Document: Onboard Hydrogen Storage for Light-Duty Fuel Cell Vehicles, U.S. Department of Energy, [https://www.energy.gov/sites/prod/files/2017/05/f34/fcto\\_targets\\_onboard\\_hydro\\_storage\\_explanation.pdf](https://www.energy.gov/sites/prod/files/2017/05/f34/fcto_targets_onboard_hydro_storage_explanation.pdf), accessed May 2020.

62. Bae, Y.-S., and Snurr, R.Q. (2010). Optimal isosteric heat of adsorption for hydrogen storage and delivery using metal–organic frameworks. *Microporous Mesoporous Mater.* *132*, 300-303.
63. Liu, Y., Eubank, J.F., Cairns, A.J., Eckert, J., Kravtsov, V.C., Luebke, R., and Eddaoudi, M. (2007). Assembly of Metal–Organic Frameworks (MOFs) Based on Indium-Trimer Building Blocks: A Porous MOF with soc Topology and High Hydrogen Storage. *Angew. Chem. Int. Ed.* *46*, 3278-3283.
64. Cairns, A.J., Eckert, J., Wojtas, L., Thommes, M., Wallacher, D., Georgiev, P.A., Forster, P.M., Belmabkhout, Y., Ollivier, J., and Eddaoudi, M. (2016). Gaining Insights on the H<sub>2</sub>–Sorbent Interactions: Robust soc-MOF Platform as a Case Study. *Chem. Mater.* *28*, 7353-7361.
65. Chen, B., Zhao, X., Putkham, A., Hong, K., Lobkovsky, E.B., Hurtado, E.J., Fletcher, A.J., and Thomas, K.M. (2008). Surface Interactions and Quantum Kinetic Molecular Sieving for H<sub>2</sub> and D<sub>2</sub> Adsorption on a Mixed Metal–Organic Framework Material. *J. Am. Chem. Soc.* *130*, 6411-6423.
66. Zhou, W., Wu, H., and Yildirim, T. (2008). Enhanced H<sub>2</sub> Adsorption in Isostructural Metal–Organic Frameworks with Open Metal Sites: Strong Dependence of the Binding Strength on Metal Ions. *J. Am. Chem. Soc.* *130*, 15268-15269.
67. Rosi, N.L., Kim, J., Eddaoudi, M., Chen, B., O’Keeffe, M., and Yaghi, O.M. (2005). Rod Packings and Metal–Organic Frameworks Constructed from Rod-Shaped Secondary Building Units. *J. Am. Chem. Soc.* *127*, 1504-1518.
68. Dietzel, P.D.C., Morita, Y., Blom, R., and Fjellvåg, H. (2005). An In Situ High-Temperature Single-Crystal Investigation of a Dehydrated Metal–Organic Framework Compound and Field-Induced Magnetization of One-Dimensional Metal–Oxygen Chains. *Angew. Chem. Int. Ed.* *44*, 6354-6358.
69. Irving, H., and Williams, R.J.P. (1948). Order of Stability of Metal Complexes. *Nature* *162*, 746-747.
70. Kapelewski, M.T., Geier, S.J., Hudson, M.R., Stück, D., Mason, J.A., Nelson, J.N., Xiao, D.J., Hulvey, Z., Gilmour, E., FitzGerald, S.A., et al. (2014). M<sub>2</sub>(m-dobdc) (M = Mg, Mn, Fe, Co, Ni) Metal–Organic Frameworks Exhibiting Increased Charge Density and Enhanced H<sub>2</sub> Binding at the Open Metal Sites. *J. Am. Chem. Soc.* *136*, 12119-12129.
71. Kapelewski, M.T., Runčevski, T., Tarver, J.D., Jiang, H.Z.H., Hurst, K.E., Parilla, P.A., Ayala, A., Gennett, T., FitzGerald, S.A., Brown, C.M., and Long, J.R. (2018). Record High Hydrogen Storage Capacity in the Metal–Organic Framework Ni<sub>2</sub>(m-dobdc) at Near-Ambient Temperatures. *Chem. Mater.* *30*, 8179-8189.
72. Denysenko, D., Grzywa, M., Tonigold, M., Streppel, B., Krkljus, I., Hirscher, M., Mugnaioli, E., Kolb, U., Hanss, J., and Volkmer, D. (2011). Elucidating Gating Effects for Hydrogen Sorption in MFU-4-Type Triazolate-Based Metal–Organic Frameworks Featuring Different Pore Sizes. *Chem. Eur. J.* *17*, 1837-1848.
73. Barnett, B.R., Evans, H.A., Su, G.M., Jiang, H.Z.H., Chakraborty, R., Banyeretse, D., Hartman, T.J., Martinez, M.B., Trump, B.A., Tarver, J.D., et al. (2021). Observation of an Intermediate to H<sub>2</sub> Binding in a Metal–Organic Framework. *J. Am. Chem. Soc.* *143*, 14884-14894.
74. Ghanem, B.S., Msayib, K.J., McKeown, N.B., Harris, K.D.M., Pan, Z., Budd, P.M., Butler, A., Selbie, J., Book, D., and Walton, A. (2007). A triptycene-based polymer of

- intrinsic microposity that displays enhanced surface area and hydrogen adsorption. *Chem. Commun.*, 67-69.
75. Zhang, Q., Cai, L., Liu, G., Li, Q., Jiang, M., and Yao, X. (2020). Selenium-Infused Ordered Mesoporous Carbon for Room-Temperature All-Solid-State Lithium–Selenium Batteries with Ultrastable Cyclability. *ACS Appl. Mater. Interfaces* *12*, 16541-16547.
  76. Langmi, H.W., Walton, A., Al-Mamouri, M.M., Johnson, S.R., Book, D., Speight, J.D., Edwards, P.P., Gameson, I., Anderson, P.A., and Harris, I.R. (2003). Hydrogen adsorption in zeolites A, X, Y and RHO. *Journal of Alloys and Compounds* *356-357*, 710-715.
  77. El-Kaderi, H.M., Hunt, J.R., Mendoza-Cortés, J.L., Côté, A.P., Taylor, R.E., Keeffe, M., and Yaghi, O.M. (2007). Designed Synthesis of 3D Covalent Organic Frameworks. *Science* *316*, 268.
  78. Tylianakis, E., Klontzas, E., and Froudakis, G.E. (2011). Multi-scale theoretical investigation of hydrogen storage in covalent organic frameworks. *Nanoscale* *3*, 856-869.
  79. Garberoglio, G. (2007). Computer Simulation of the Adsorption of Light Gases in Covalent Organic Frameworks. *Langmuir* *23*, 12154-12158.
  80. Furukawa, H., and Yaghi, O.M. (2009). Storage of Hydrogen, Methane, and Carbon Dioxide in Highly Porous Covalent Organic Frameworks for Clean Energy Applications. *J. Am. Chem. Soc.* *131*, 8875-8883.
  81. Klontzas, E., Tylianakis, E., and Froudakis, G.E. (2008). Hydrogen Storage in 3D Covalent Organic Frameworks. A Multiscale Theoretical Investigation. *J. Phys. Chem. C* *112*, 9095-9098.
  82. Cao, D., Lan, J., Wang, W., and Smit, B. (2009). Lithium-Doped 3D Covalent Organic Frameworks: High-Capacity Hydrogen Storage Materials. *Angew. Chem. Int. Ed.* *48*, 4730-4733.
  83. Klontzas, E., Tylianakis, E., and Froudakis, G.E. (2009). Hydrogen Storage in Lithium-Functionalized 3-D Covalent-Organic Framework Materials. *J. Phys. Chem. C* *113*, 21253-21257.
  84. Li, F., Zhao, J., Johansson, B., and Sun, L. (2010). Improving hydrogen storage properties of covalent organic frameworks by substitutional doping. *Int. J. Hydrogen Energy* *35*, 266-271.
  85. Germain, J., Fréchet, J.M.J., and Svec, F. (2009). Nanoporous Polymers for Hydrogen Storage. *Small* *5*, 1098-1111.
  86. Jiang, J.-X., Su, F., Niu, H., Wood, C.D., Campbell, N.L., Khimyak, Y.Z., and Cooper, A.I. (2008). Conjugated microporous poly(phenylene butadiynylene)s. *Chem. Commun.*, 486-488.
  87. Yuan, S., Dorney, B., White, D., Kirklin, S., Zapol, P., Yu, L., and Liu, D.-J. (2010). Microporous polyphenylenes with tunable pore size for hydrogen storage. *Chem. Commun.* *46*, 4547-4549.
  88. Chen, Q., Wang, J.-X., Yang, F., Zhou, D., Bian, N., Zhang, X.-J., Yan, C.-G., and Han, B.-H. (2011). Tetraphenylethylene-based fluorescent porous organic polymers: preparation, gas sorption properties and photoluminescence properties. *J. Mater. Chem.* *21*, 13554-13560.
  89. Qiao, S., Du, Z., and Yang, R. (2014). Design and synthesis of novel carbazole–spacer–carbazole type conjugated microporous networks for gas storage and separation. *J. Mater. Chem. A* *2*, 1877-1885.

90. Ben, T., Ren, H., Ma, S., Cao, D., Lan, J., Jing, X., Wang, W., Xu, J., Deng, F., Simmons, J.M., et al. (2009). Targeted Synthesis of a Porous Aromatic Framework with High Stability and Exceptionally High Surface Area. *Angew. Chem. Int. Ed.* *48*, 9457-9460.
91. Yuan, D., Lu, W., Zhao, D., and Zhou, H.-C. (2011). Highly Stable Porous Polymer Networks with Exceptionally High Gas-Uptake Capacities. *Adv. Mater.* *23*, 3723-3725.
92. Polak-Kraśna, K., Dawson, R., Holyfield, L.T., Bowen, C.R., Burrows, A.D., and Mays, T.J. (2017). Mechanical characterisation of polymer of intrinsic microporosity PIM-1 for hydrogen storage applications. *Journal of Materials Science* *52*, 3862-3875.
93. Rochat, S., Polak-Kraśna, K., Tian, M., Mays, T.J., Bowen, C.R., and Burrows, A.D. (2019). Assessment of the long-term stability of the polymer of intrinsic microporosity PIM-1 for hydrogen storage applications. *Int. J. Hydrogen Energy* *44*, 332-337.
94. Bera, R., Mondal, S., and Das, N. (2018). Triptycene based microporous polymers (TMPs): Efficient small gas (H<sub>2</sub> and CO<sub>2</sub>) storage and high CO<sub>2</sub>/N<sub>2</sub> selectivity. *Microporous Mesoporous Mater.* *257*, 253-261.
95. Titirici, M.-M., White, R.J., Brun, N., Budarin, V.L., Su, D.S., del Monte, F., Clark, J.H., and MacLachlan, M.J. (2015). Sustainable carbon materials. *Chem. Soc. Rev.* *44*, 250-290.
96. Hirscher, M., Yartys, V.A., Baricco, M., Bellosta von Colbe, J., Blanchard, D., Bowman, R.C., Broom, D.P., Buckley, C.E., Chang, F., Chen, P., et al. (2020). Materials for hydrogen-based energy storage – past, recent progress and future outlook. *Journal of Alloys and Compounds* *827*, 153548.
97. Sawant, S.Y., Munusamy, K., Somani, R.S., John, M., Newalkar, B.L., and Bajaj, H.C. (2017). Precursor suitability and pilot scale production of super activated carbon for greenhouse gas adsorption and fuel gas storage. *Chem. Eng. J.* *315*, 415-425.
98. Ryoo, R., Joo, S.H., Kruk, M., and Jaroniec, M. (2001). Ordered Mesoporous Carbons. *Adv. Mater.* *13*, 677-681.
99. Nishihara, H., and Kyotani, T. (2012). Templated Nanocarbons for Energy Storage. *Adv. Mater.* *24*, 4473-4498.
100. Liu, B., Shioyama, H., Akita, T., and Xu, Q. (2008). Metal-Organic Framework as a Template for Porous Carbon Synthesis. *J. Am. Chem. Soc.* *130*, 5390-5391.
101. Ryoo, R., Joo, S.H., and Jun, S. (1999). Synthesis of Highly Ordered Carbon Molecular Sieves via Template-Mediated Structural Transformation. *J. Phys. Chem. B* *103*, 7743-7746.
102. Lee, J., Yoon, S., Hyeon, T., M. Oh, S., and Bum Kim, K. (1999). Synthesis of a new mesoporous carbon and its application to electrochemical double-layer capacitors. *Chem. Commun.*, 2177-2178.
103. Ma, Z., Kyotani, T., and Tomita, A. (2000). Preparation of a high surface area microporous carbon having the structural regularity of Y zeolite. *Chem. Commun.*, 2365-2366.
104. Johnson, S.A., Brigham, E.S., Ollivier, P.J., and Mallouk, T.E. (1997). Effect of Micropore Topology on the Structure and Properties of Zeolite Polymer Replicas. *Chem. Mater.* *9*, 2448-2458.
105. Kyotani, T., Nagai, T., Inoue, S., and Tomita, A. (1997). Formation of New Type of Porous Carbon by Carbonization in Zeolite Nanochannels. *Chem. Mater.* *9*, 609-615.

106. Rodriguez-Mirasol, J., Cordero, T., Radovic, L.R., and Rodriguez, J.J. (1998). Structural and Textural Properties of Pyrolytic Carbon Formed within a Microporous Zeolite Template. *Chem. Mater.* *10*, 550-558.
107. Pang, J., Hampsey, J.E., Wu, Z., Hu, Q., and Lu, Y. (2004). Hydrogen adsorption in mesoporous carbons. *Appl. Phys. Lett.* *85*, 4887-4889.
108. Gadiou, R., Saadallah, S.-E., Piquero, T., David, P., Parmentier, J., and Vix-Guterl, C. (2005). The influence of textural properties on the adsorption of hydrogen on ordered nanostructured carbons. *Microporous Mesoporous Mater.* *79*, 121-128.
109. Oschatz, M., Kockrick, E., Rose, M., Borchardt, L., Klein, N., Senkovska, I., Freudenberg, T., Korenblit, Y., Yushin, G., and Kaskel, S. (2010). A cubic ordered, mesoporous carbide-derived carbon for gas and energy storage applications. *Carbon* *48*, 3987-3992.
110. Xia, K., Gao, Q., Song, S., Wu, C., Jiang, J., Hu, J., and Gao, L. (2008). CO<sub>2</sub> activation of ordered porous carbon CMK-1 for hydrogen storage. *Int. J. Hydrogen Energy* *33*, 116-123.
111. Armandi, M., Bonelli, B., Karaindrou, E.I., Areán, C.O., and Garrone, E. (2008). Post-synthesis modifications of SBA-15 carbon replicas: Improving hydrogen storage by increasing microporous volume. *Catalysis Today* *138*, 244-248.
112. Yang, Z., Xia, Y., and Mokaya, R. (2007). Enhanced Hydrogen Storage Capacity of High Surface Area Zeolite-like Carbon Materials. *J. Am. Chem. Soc.* *129*, 1673-1679.
113. Zhu, Z.H., Lu, G.Q., and Hatori, H. (2006). New Insights into the Interaction of Hydrogen Atoms with Boron-Substituted Carbon. *J. Phys. Chem. B* *110*, 1249-1255.
114. Aijaz, A., Akita, T., Yang, H., and Xu, Q. (2014). From ionic-liquid@metal-organic framework composites to heteroatom-decorated large-surface area carbons: superior CO<sub>2</sub> and H<sub>2</sub> uptake. *Chem. Commun.* *50*, 6498-6501.
115. Blankenship Ii, T.S., Balahmar, N., and Mokaya, R. (2017). Oxygen-rich microporous carbons with exceptional hydrogen storage capacity. *Nat. Commun.* *8*, 1545.
116. Wang, L., and Yang, R.T. (2008). New sorbents for hydrogen storage by hydrogen spillover – a review. *Energy Environ. Sci.* *1*, 268-279.
117. Streb, A., and Mazzotti, M. (2021). Adsorption for efficient low carbon hydrogen production: part 1—adsorption equilibrium and breakthrough studies for H<sub>2</sub>/CO<sub>2</sub>/CH<sub>4</sub> on zeolite 13X. *Adsorption* *27*, 541-558.
118. Gutowska, A., Li, L., Shin, Y., Wang, C.M., Li, X.S., Linehan, J.C., Smith, R.S., Kay, B.D., Schmid, B., Shaw, W., et al. (2005). Nanoscaffold Mediates Hydrogen Release and the Reactivity of Ammonia Borane. *Angew. Chem. Int. Ed.* *44*, 3578-3582.
119. Ngene, P., Adelhelm, P., Beale, A.M., de Jong, K.P., and de Jongh, P.E. (2010). LiBH<sub>4</sub>/SBA-15 Nanocomposites Prepared by Melt Infiltration under Hydrogen Pressure: Synthesis and Hydrogen Sorption Properties. *J. Phys. Chem. C* *114*, 6163-6168.
120. Suwarno, Ngene, P., Nale, A., Eggenhuisen, T.M., Oschatz, M., Embs, J.P., Remhof, A., and de Jongh, P.E. (2017). Confinement Effects for Lithium Borohydride: Comparing Silica and Carbon Scaffolds. *J. Phys. Chem. C* *121*, 4197-4205.
121. Xia, G., Li, L., Guo, Z., Gu, Q., Guo, Y., Yu, X., Liu, H., and Liu, Z. (2013). Stabilization of NaZn(BH<sub>4</sub>)<sub>3</sub> via nanoconfinement in SBA-15 towards enhanced hydrogen release. *J. Mater. Chem. A* *1*, 250-257.

122. Yao, Q., Lu, Z.-H., Yang, K., Chen, X., and Zhu, M. (2015). Ruthenium nanoparticles confined in SBA-15 as highly efficient catalyst for hydrolytic dehydrogenation of ammonia borane and hydrazine borane. *Sci. Rep.* *5*, 15186.
123. Cho, Y., Li, S., Snider, J.L., Marple, M.A.T., Strange, N.A., Sugar, J.D., El Gabaly, F., Schneemann, A., Kang, S., Kang, M.-h., et al. (2021). Reversing the Irreversible: Thermodynamic Stabilization of LiAlH<sub>4</sub> Nanoconfined Within a Nitrogen-Doped Carbon Host. *ACS Nano* *15*, 10163-10174.
124. Liu, X., Peaslee, D., Jost, C.Z., and Majzoub, E.H. (2010). Controlling the Decomposition Pathway of LiBH<sub>4</sub> via Confinement in Highly Ordered Nanoporous Carbon. *J. Phys. Chem. C* *114*, 14036-14041.
125. Liu, X., Peaslee, D., Jost, C.Z., Baumann, T.F., and Majzoub, E.H. (2011). Systematic Pore-Size Effects of Nanoconfinement of LiBH<sub>4</sub>: Elimination of Diborane Release and Tunable Behavior for Hydrogen Storage Applications. *Chem. Mater.* *23*, 1331-1336.
126. Gasnier, A., and Gennari, F.C. (2017). Graphene entanglement in a mesoporous resorcinol–formaldehyde matrix applied to the nanoconfinement of LiBH<sub>4</sub> for hydrogen storage. *RSC Adv.* *7*, 27905-27912.
127. Wu, R., Zhang, X., Liu, Y., Zhang, L., Hu, J., Gao, M., and Pan, H. (2020). A Unique Double-Layered Carbon Nanobowl-Confined Lithium Borohydride for Highly Reversible Hydrogen Storage. *Small* *16*, 2001963.
128. Lai, Q., Yang, Y., and Aguey-Zinsou, K.-F. (2019). Nanoconfinement of borohydrides in hollow carbon spheres: Melt infiltration versus solvent impregnation for enhanced hydrogen storage. *Int. J. Hydrogen Energy* *44*, 23225-23238.
129. Lai, Q., Prathana, C., Yang, Y., Rawal, A., and Aguey-Zinsou, K.-F. (2021). Nanoconfinement of Complex Borohydrides for Hydrogen Storage. *ACS Appl. Nano Mater.* *4*, 973-978.
130. Zheng, J., Yao, Z., Xiao, X., Wang, X., He, J., Chen, M., Cheng, H., Zhang, L., and Chen, L. (2021). Enhanced hydrogen storage properties of high-loading nanoconfined LiBH<sub>4</sub>–Mg(BH<sub>4</sub>)<sub>2</sub> composites with porous hollow carbon nanospheres. *Int. J. Hydrogen Energy* *46*, 852-864.
131. Gross, A.F., Vajo, J.J., Van Atta, S.L., and Olson, G.L. (2008). Enhanced Hydrogen Storage Kinetics of LiBH<sub>4</sub> in Nanoporous Carbon Scaffolds. *J. Phys. Chem. C* *112*, 5651-5657.
132. Li, Y.-T., Zhang, X.-L., Peng, Z.-K., Liu, P., and Zheng, X.-C. (2020). Hierarchical Porous g-C<sub>3</sub>N<sub>4</sub> Coupled Ultrafine RuNi Alloys as Extremely Active Catalysts for the Hydrolytic Dehydrogenation of Ammonia Borane. *ACS Sustain Chem Eng.* *8*, 8458-8468.
133. Wahab, M.A., Young, D.J., Karim, A., Fawzia, S., and Beltramini, J.N. (2016). Low-temperature hydrogen desorption from Mg(BH<sub>4</sub>)<sub>2</sub> catalysed by ultrafine Ni nanoparticles in a mesoporous carbon matrix. *Int. J. Hydrogen Energy* *41*, 20573-20582.
134. Mao, M., Chen, Q., Wu, J., and Fan, G. (2020). Anchoring and space-confinement effects to synthesize ultrasmall Pd nanoparticles for efficient ammonia borane hydrolysis. *Int. J. Hydrogen Energy* *45*, 27244-27253.
135. Xian, K., Nie, B., Li, Z., Gao, M., Li, Z., Shang, C., Liu, Y., Guo, Z., and Pan, H. (2021). TiO<sub>2</sub> decorated porous carbonaceous network structures offer confinement, catalysis and thermal conductivity for effective hydrogen storage of LiBH<sub>4</sub>. *Chem. Eng. J.* *407*, 127156.

136. Ding, R., Chen, Q., Luo, Q., Zhou, L., Wang, Y., Zhang, Y., and Fan, G. (2020). Salt template-assisted in situ construction of Ru nanoclusters and porous carbon: excellent catalysts toward hydrogen evolution, ammonia-borane hydrolysis, and 4-nitrophenol reduction. *Green Chem.* *22*, 835-842.
137. Wang, S., Gao, M., Yao, Z., Liu, Y., Wu, M., Li, Z., Liu, Y., Sun, W., and Pan, H. (2022). A nanoconfined-LiBH<sub>4</sub> system using a unique multifunctional porous scaffold of carbon wrapped ultrafine Fe<sub>3</sub>O<sub>4</sub> skeleton for reversible hydrogen storage with high capacity. *Chem. Eng. J.* *428*, 131056.
138. Liu, H., Jiao, L., Zhao, Y., Cao, K., Liu, Y., Wang, Y., and Yuan, H. (2014). Improved dehydrogenation performance of LiBH<sub>4</sub> by confinement into porous TiO<sub>2</sub> micro-tubes. *J. Mater. Chem. A* *2*, 9244-9250.
139. Leick, N., Strange, N.A., Schneemann, A., Stavila, V., Gross, K., Washton, N., Settle, A., Martinez, M.B., Gennett, T., and Christensen, S.T. (2021). Al<sub>2</sub>O<sub>3</sub> Atomic Layer Deposition on Nanostructured  $\gamma$ -Mg(BH<sub>4</sub>)<sub>2</sub> for H<sub>2</sub> Storage. *ACS Applied Energy Materials* *4*, 1150-1162.
140. Feng, Y., Zhou, X., Yang, J.-h., Gao, X., Yin, L., Zhao, Y., and Zhang, B. (2020). Encapsulation of Ammonia Borane in Pd/Halloysite Nanotubes for Efficient Thermal Dehydrogenation. *ACS Sustain Chem Eng.* *8*, 2122-2129.
141. Schneemann, A., White, J.L., Kang, S., Jeong, S., Wan, L.F., Cho, E.S., Heo, T.W., Prendergast, D., Urban, J.J., Wood, B.C., et al. (2018). Nanostructured Metal Hydrides for Hydrogen Storage. *Chem. Rev.* *118*, 10775-10839.
142. Stavila, V., Bhakta, R.K., Alam, T.M., Majzoub, E.H., and Allendorf, M.D. (2012). Reversible Hydrogen Storage by NaAlH<sub>4</sub> Confined within a Titanium-Functionalized MOF-74(Mg) Nanoreactor. *ACS Nano* *6*, 9807-9817.
143. Bhakta, R.K., Herberg, J.L., Jacobs, B., Highley, A., Behrens, R., Ockwig, N.W., Greathouse, J.A., and Allendorf, M.D. (2009). Metal–Organic Frameworks As Templates for Nanoscale NaAlH<sub>4</sub>. *J. Am. Chem. Soc.* *131*, 13198-13199.
144. Jeong, H.M., Shin, W.H., Park, J.H., Choi, J.H., and Kang, J.K. (2014). A metal–organic framework as a chemical guide to control hydrogen desorption pathways of ammonia borane. *Nanoscale* *6*, 6526-6530.
145. Li, Z., Zhu, G., Lu, G., Qiu, S., and Yao, X. (2010). Ammonia Borane Confined by a Metal–Organic Framework for Chemical Hydrogen Storage: Enhancing Kinetics and Eliminating Ammonia. *J. Am. Chem. Soc.* *132*, 1490-1491.
146. Gadipelli, S., Ford, J., Zhou, W., Wu, H., Udovic, T.J., and Yildirim, T. (2011). Nanoconfinement and Catalytic Dehydrogenation of Ammonia Borane by Magnesium-Metal–Organic-Framework-74. *Chem. Eur. J.* *17*, 6043-6047.
147. Srinivas, G., Travis, W., Ford, J., Wu, H., Guo, Z.-X., and Yildirim, T. (2013). Nanoconfined ammonia borane in a flexible metal–organic framework Fe–MIL-53: clean hydrogen release with fast kinetics. *J. Mater. Chem. A* *1*, 4167-4172.
148. Si, X.-l., Sun, L.-x., Xu, F., Jiao, C.-l., Li, F., Liu, S.-s., Zhang, J., Song, L.-f., Jiang, C.-h., Wang, S., et al. (2011). Improved hydrogen desorption properties of ammonia borane by Ni-modified metal-organic frameworks. *Int. J. Hydrogen Energy* *36*, 6698-6704.
149. Carr, C.L., Jayawardana, W., Zou, H., White, J.L., El Gabaly, F., Conradi, M.S., Stavila, V., Allendorf, M.D., and Majzoub, E.H. (2018). Anomalous H<sub>2</sub> Desorption Rate of NaAlH<sub>4</sub> Confined in Nitrogen-Doped Nanoporous Carbon Frameworks. *Chem. Mater.* *30*, 2930-2938.

150. Carr, C.L., and Majzoub, E.H. (2016). Surface-Functionalized Nanoporous Carbons for Kinetically Stabilized Complex Hydrides through Lewis Acid–Lewis Base Chemistry. *J. Phys. Chem. C* *120*, 11426-11432.
151. Ma, Z., Zhang, Q., Panda, S., Zhu, W., Sun, F., Khan, D., Dong, J., Ding, W., and Zou, J. (2020). In situ catalyzed and nanoconfined magnesium hydride nanocrystals in a Ni-MOF scaffold for hydrogen storage. *Sustainable Energy & Fuels* *4*, 4694-4703.
152. Zhao-Karger, Z., Hu, J., Roth, A., Wang, D., Kübel, C., Lohstroh, W., and Fichtner, M. (2010). Altered thermodynamic and kinetic properties of MgH<sub>2</sub> infiltrated in microporous scaffold. *Chem. Commun.* *46*, 8353-8355.
153. Peil, S., Wissler, D., Stähle, M., Roßmann, P.K., Avadhut, Y.S., and Hartmann, M. (2021). Hydrogen Release from Ammonia Borane Nanoconfined in Metal–Organic Frameworks with MIL-53 Topology. *J. Phys. Chem. C* *125*, 9990-10000.
154. Metal-Organic Frameworks: Mechanochemical Synthesis Strategies. In *Encyclopedia of Inorganic and Bioinorganic Chemistry*, pp. 1-19. 10.1002/9781119951438.eibc2202.
155. Al-Kutubi, H., Gascon, J., Sudhölter, E.J.R., and Rassaei, L. (2015). Electrosynthesis of Metal–Organic Frameworks: Challenges and Opportunities. *ChemElectroChem* *2*, 462-474.
156. Duan, C., Yu, Y., Xiao, J., Zhang, X., Li, L., Yang, P., Wu, J., and Xi, H. (2020). Water-based routes for synthesis of metal-organic frameworks: A review. *Sci. China Mater.* *63*, 667-685.
157. Anastasopoulou, A., Furukawa, H., Barnett, B.R., Jiang, H.Z.H., Long, J.R., and Breunig, H.M. (2021). Technoeconomic analysis of metal–organic frameworks for bulk hydrogen transportation. *Energy Environ. Sci.* *14*, 1083-1094.

**Figure 1.** An overview of hydrogen storage using metal–organic frameworks.

**Figure 2.** Crystal structures of selected MOFs and their deliverable capacities under the operating conditions (77 K/100 bar → 160 K/5 bar).

**Figure 3.** Structures of (A) MOF-74 and (B) M<sub>2</sub>(*m*-dobdc). (C) The isosteric heat of adsorption of H<sub>2</sub> for M<sub>2</sub>(*m*-dobdc). (D) The comparison of M–D<sub>2</sub> distance for Co<sub>2</sub>(dobdc) and Co<sub>2</sub>(*m*-dobdc) revealed by neutron diffraction experiments. Figures C and D are adapted with permission from Kapelewski et al<sup>70</sup>. Copyright 2014 American Chemical Society.

**Figure 4.** Structures, respective inorganic building units, and isosteric heats of adsorption for H<sub>2</sub> of (A) Cu<sup>I</sup>-MFU-4l<sup>29</sup> and (B) V<sub>2</sub>Cl<sub>2.8</sub>(btdd)<sup>30</sup>.

**Figure 5.** An overview figure showing the advantages and disadvantages of all materials and selected materials' performance towards hydrogen storage. The representative figures of COFs, POPs, carbon-based materials, and zeolites are reprinted with permission from Côté et al.<sup>17</sup> Copyright 2005 American Association for the Advancement of Science, Ghanem et al.<sup>74</sup> Copyright 2007 Royal Society of Chemistry, Zhang et al.<sup>75</sup> Copyright 2020 American Chemical Society, Langmi et al.<sup>76</sup> Copyright 2003 Elsevier, respectively.

**Figure 6.** Benefits of nanoconfinement of HLEs in porous materials. (A) describes the four different classes of HLEs. (B) describes drawbacks of using bulk HLEs. (C) shows advantages of confinement of HLEs within porous materials.

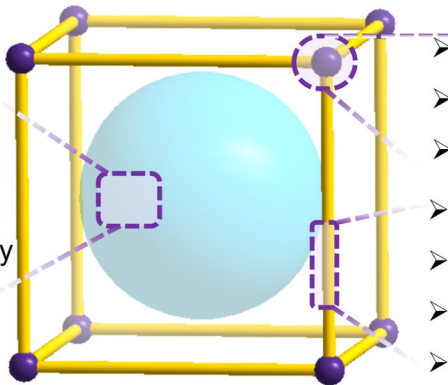
**Table 1.** Gravimetric and volumetric BET area, pore volume (PV), crystallographic density, topological nets, and H<sub>2</sub> working performance for selected highly porous MOFs.<sup>a</sup>

Materials	BET area (m <sup>2</sup> g <sup>-1</sup> )	PV (cm <sup>3</sup> g <sup>-1</sup> )	Density (g cm <sup>-3</sup> ) <sup>b</sup>	Vol. BET area <sup>c</sup> (m <sup>2</sup> cm <sup>-3</sup> )	Nets	$\Delta H_2$ @(77 K/100 bar → 160 K/5 bar)		Q <sub>st</sub> (kJ mol <sup>-1</sup> )	Ref.
						wt%	g L <sup>-1</sup>		
MOF-5	3510	1.36	0.59	2070	pcu	7.8	51.9	-	51
IRMOF-20	4070	1.65	0.51	2080	pcu	9.1	51	-	51
NU-1101	4340	1.72	0.459	1990	ftw	9.1	46.6	5.5	54
NU-1102	3720	1.65	0.403	1500	ftw	9.6	43.7	4.5	54
NU-1103	6245	2.72	0.298	1860	ftw	12.6	43.2	3.8	54
SNU-70	4940	2.14	0.411	2030	pcu	10.6	47.9	-	28
UMCM-9	5040	2.31	0.37	1860	pcu	11.3	47.4	-	28
NU-100/PCN-610	6050	3.17	0.29	1755	rht	13.9	47.6	-	28
NPF-200	5830	2.17	0.389	2268	-	11.4	49.8	4.5	55
NU-1500-Al	3560	1.46	0.498	1770	acs	8.2	44.6	4.9	27
NU-1501-Fe	7140	2.90	0.299	2130	acs	13.2	45.4	4	27
NU-1501-Al	7310	2.91	0.283	2060	acs	14.0	46.2	4	27

<b>MFU-4l-Li</b>	4070	1.66	0.479	1950	<b>pcu</b>	9.4	50.2	5.4	<sup>56</sup>
------------------	------	------	-------	------	------------	-----	------	-----	---------------

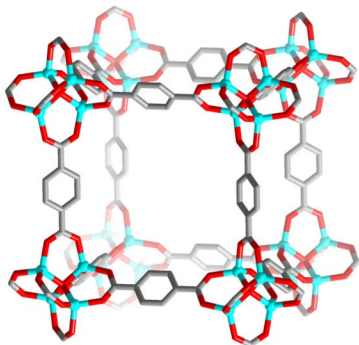
<sup>a</sup> Related values are obtained from the reported literature. The H<sub>2</sub> capacity in wt% is calculated according to  $\text{wt\%} = (\text{mass of H}_2) / (\text{mass of H}_2 + \text{mass of MOF}) \times 100\%$ . <sup>b</sup> Crystallographic density is calculated from crystal structures or optimized structure. <sup>c</sup> Volumetric BET area is calculated based on crystallographic density.

- High porosity
- High surface area
- Tunable pore size
- Controllable pore geometry
- Functional guests



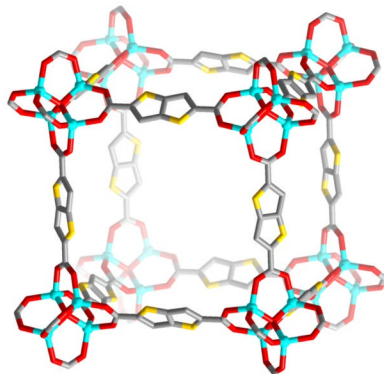
- Inorganic building units
- Open metal sites
- Backbonding interaction
- Organic ligands
- Isoreticular expansion/contraction
- Functionalities
- Amenable to post-modification

**Metal–organic frameworks (MOFs)**



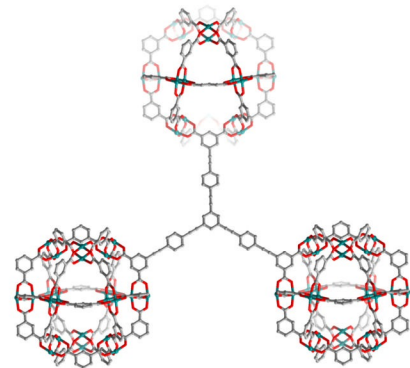
**MOF-5**

7.8 wt% and 51.9 g L<sup>-1</sup>



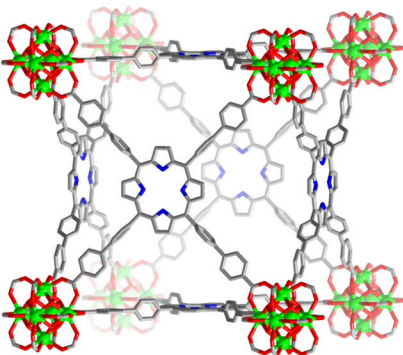
**IRMOF-20**

9.1 wt% and 51 g L<sup>-1</sup>



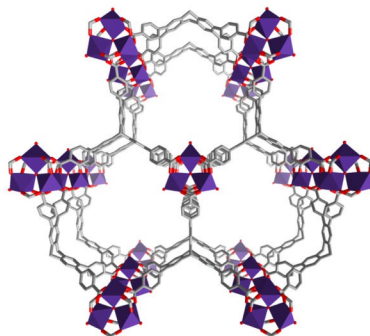
**NU-100/PCN-610**

13.9 wt% and 47.6 g L<sup>-1</sup>



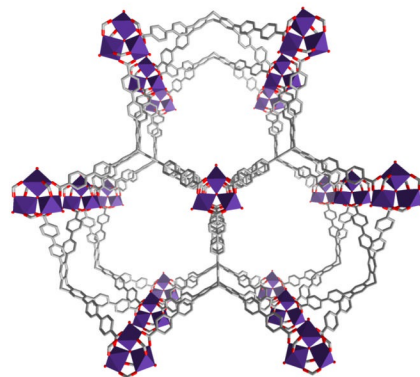
**NU-1102**

9.6 wt% and 43.7 g L<sup>-1</sup>



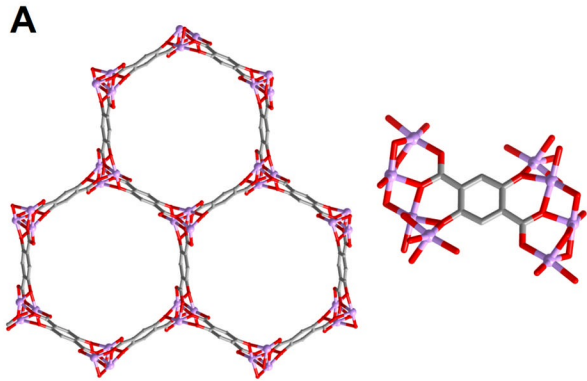
**NU-1500-AI**

8.2 wt% and 44.6 g L<sup>-1</sup>

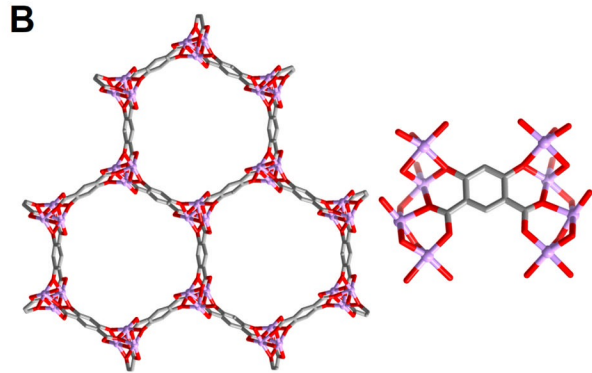


**NU-1501-AI**

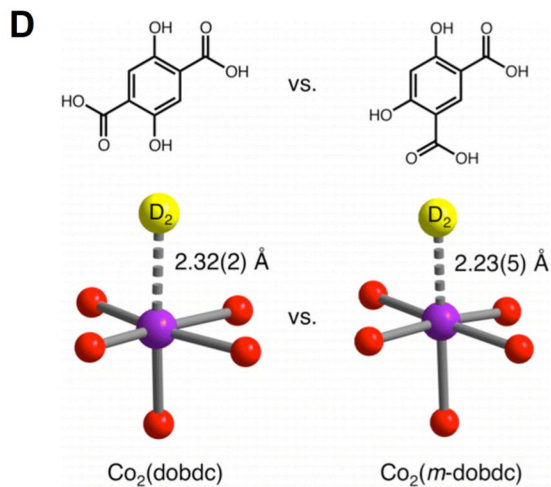
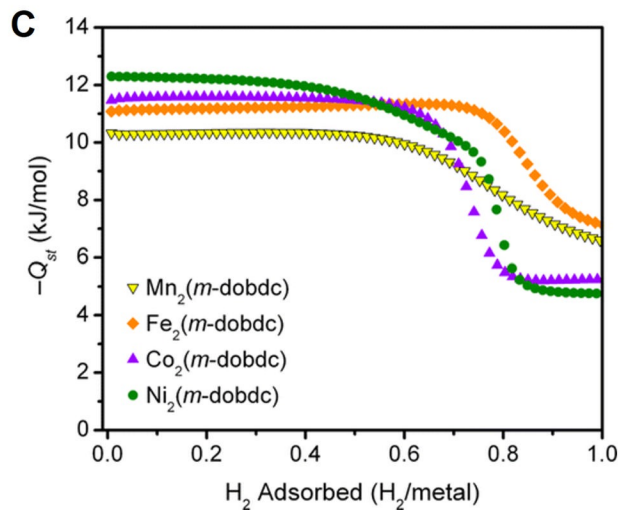
14.0 wt% and 46.2 g L<sup>-1</sup>

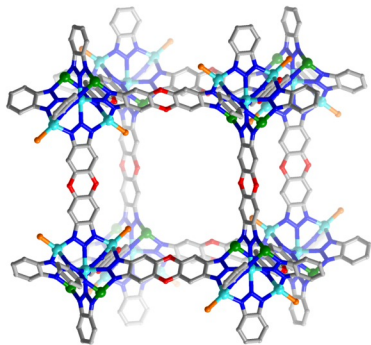


$M_2(\text{dobdc})/\text{M-MOF-74}/\text{CPO-27-M}$

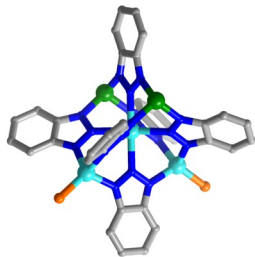


$M_2(m\text{-dobdc})$

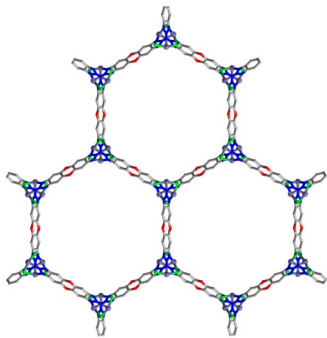


**A**

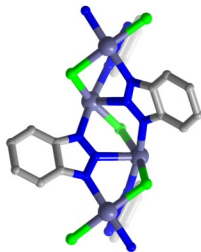
$\text{Cu}^{\text{I}}\text{-MFU-4l}$



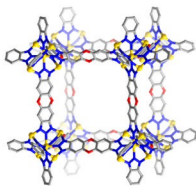
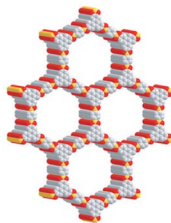
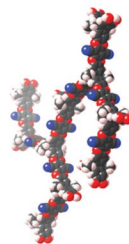
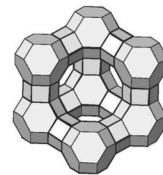
Isosteric heat of adsorption  
=  $-32 \text{ kJ mol}^{-1}$

**B**

$\text{V}_2\text{Cl}_{2.8}(\text{btdd})$



Isosteric heat of adsorption  
=  $-21 \text{ kJ mol}^{-1}$

**Metal-organic frameworks****Covalent organic frameworks****Porous organic polymers****Carbon-based materials****Zeolites****Advantages**

- High crystallinity;
- High surface area and pore volume;
- Tunable structures and properties;
- Designability;
- Rich open metal sites

- Crystallinity;
- Good surface area and pore volume;
- Tunable chemical properties;
- Structural diversity

- Dynamic structures;
- Chemical and structural diversity
- Chemical and water stability

- High thermal and chemical stability;
- Ease of processibility;
- Inexpensive

- High crystallinity;
- Thermal and hydrolytic stability;
- Inexpensive

**Disadvantages**

- Low H<sub>2</sub> uptake at ambient temperatures
- Processibility

- Lack of binding sites for H<sub>2</sub>
- Difficulty of activation
- Processibility

- Lack of binding sites for H<sub>2</sub>
- Amorphous
- Non-uniform pore sizes

- Lack of binding sites for H<sub>2</sub>;
- Non-uniform pore sizes;
- Hard to control the pore structure

- Lack of binding sites for H<sub>2</sub>;
- Limited structural diversity;
- Low gravimetric hydrogen uptake
- Tunability

**77K/100bar→160K/5bar**

NU-1501-Al  
14 wt%/46.2 g L<sup>-1</sup>

**298K 100bar→5bar**

Ni<sub>2</sub>(m-dobdc)  
1.9 wt%/11 g L<sup>-1</sup>

**77K 85bar→5bar**  
COF-103

6.4 wt%/29.2 g L<sup>-1</sup>

**77K /48 bar**

PAF-1

7.0 wt% (excess)

**77K /100 bar**

PIM-1  
2.6 wt%

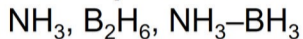
**77K 85bar→5bar**  
BPL carbon  
1.86 wt%/16.5 g L<sup>-1</sup>

**77K /15 bar**  
NaX  
1.79 wt%

**Selected materials' performance**

## A Classes of HLEs:

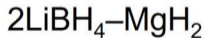
### **Simple HLEs**



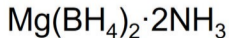
### **Metalated HLEs**



### **Composites**



### **Complexes**



## B Drawbacks with bulk HLEs:

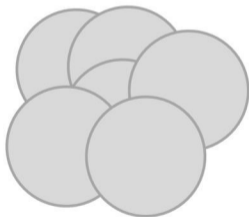


1. High temp

2. Irreversible

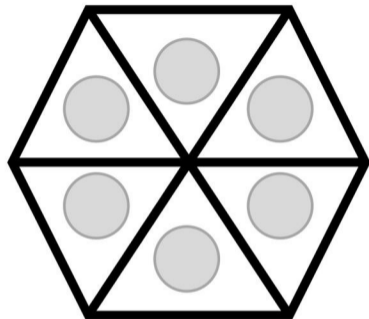
3. Large particles;  
poor kinetics

4. By-product formation

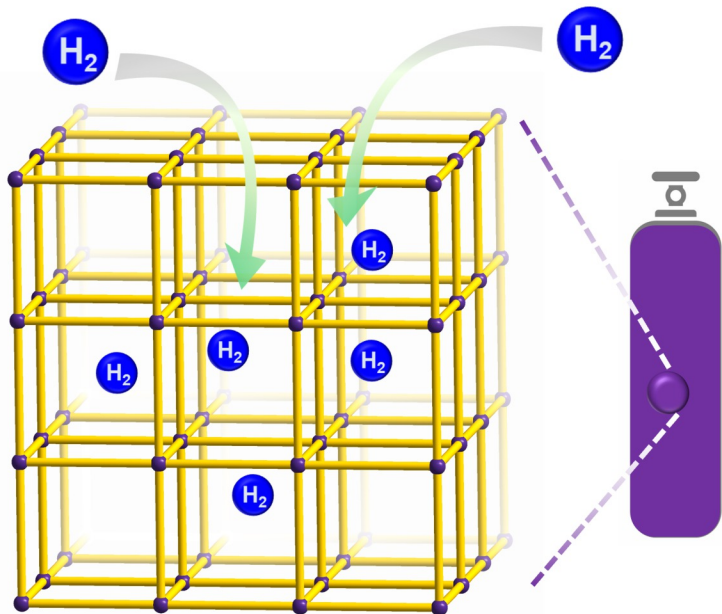


5. Aggregation upon  
cycling

## C HLE Confinement in Porous Materials



- Improved kinetics
- Reversible  $\text{H}_2$  desorption at lower temps w/ fewer by-products
- Highly tunable porous scaffolds available



**Porous Materials for Hydrogen Storage**